Purine Biosynthesis Pathways Are Required for Myogenesis in Xenopus laevis

Maëlle Duperray, Fanny Hardet, Elodie Henriet, Christelle Saint-Marc, Eric Boué-Grabot, Bertrand Daignan-Fornier, Karine Massé, Benoît Pinson

Purine biosynthesis pathways are required for myogenesis in *Xenopus laevis*

Maëlle Duperray[1], Fanny Hardet[2], Elodie Henriet[2], Christelle Saint-Marc[1,3], Eric Boué-Grabot[2], Bertrand Daignan-Fornier[1], Karine Massé[2,4*] and Benoît Pinson[1,4*]

[1] Université de Bordeaux, Institut de Biochimie et Génétique Cellulaires CNRS UMR 5095, Bordeaux, France

[2] Université de Bordeaux, CNRS, IMN, UMR 5293, F-33000 Bordeaux, France

[3]Present address: CRISP'edit platform TBMCore – Université de Bordeaux - CNRS UAR 3427 - INSERM US005, 146 rue Leo Saignat 33000 Bordeaux France

[4] Senior co-authors

*Corresponding authors: karine.masse@u-bordeaux.fr; benoit.pinson@ibgc.cnrs.fr

Abstract

Purines are required for fundamental biological processes and alterations in their metabolism lead to severe genetic diseases associated with developmental defects whose etiology remains unclear. Here, we studied the developmental requirements for purine metabolism using the amphibian *Xenopus laevis* as a vertebrate model. We provide the first functional characterization of purine pathway-genes and show that these genes are mainly expressed in nervous and muscular embryonic tissues. Morphants were generated to decipher the functions of these genes, with a focus on the adenylosuccinate lyase (*ADSL*), an enzyme required for both salvage and *de novo* purine pathways. *adsl.L* knock-down leads to severe reduction in the expression of the Myogenic Regulatory Factors (MRFs: Myod1, Myf5 and Myogenin), thus resulting in defects in somite formation and at later stages development and/or migration of both craniofacial and hypaxial muscle progenitors. Reduced expression of *hprt1.L* and *ppat*, two genes specific to the salvage and the *de novo* pathways, respectively, resulted in similar alterations. In conclusion, our data shows for the first time that *de novo* and recycling purine pathways are essential for myogenesis and highlight new mechanisms in the regulation of MRFs gene expression.

1. Introduction

Purine triphosphate nucleotides, ATP and GTP are synthesized via a highly conserved [1] *de novo* pathway allowing sequential construction of the purine ring on a ribose phosphate moiety provided by phosphoribosyl pyrophosphate (PRPP) (Figure 1A and Figure S1 for details). This *de novo* pathway results in the synthesis of inosine 5'-monophosphate (IMP) that can be converted into either AMP or GMP and then into other phosphorylated nucleotide forms required for all known forms of life. These nucleotides can alternatively be synthetized *via* a salvage pathway using precursors taken up from the extracellular medium or coming from the internal recycling of preexisting purines (Figure 1A). Purines and their derivatives (such as NAD(P) (nicotinamide adenine dinucleotide (phosphate)), FAD (Flavin adenine dinucleotide), coenzyme A, ADP-ribose, S-adenosyl-methionine and S-adenosyl-homocysteine) form a family of metabolites among the most abundant (mM range) in cells and are involved in a myriad of physiological events. Purines are required for numerous cellular processes such as biosynthesis of nucleic acids and lipids, replication, transcription, translation, maintenance of energy and redox balances, regulation of gene expression (methylation, acetylation…) and cell signaling, such as the purinergic signaling pathway [2]. Therefore, defects, even minor, in the purine *de novo* biosynthesis or recycling pathways lead to deleterious physiological effects. Indeed, to date, no less than 35 rare genetic pathologies have been associated with purine metabolism dysfunctions [3–7].

Purine-associated pathologies share a broad spectrum of clinical symptoms including hyperuricemia, immunological, hematological and renal manifestations and severe muscular and neurological dysfunctions [3,4]. They are all characterized by abnormal levels of purine nucleotides, nucleosides and/or nucleobases in the patient's body fluids and/or cells. Although in most cases the mutated gene has been identified, the causal link between the defective enzyme, the decrease in some final products, the accumulation of purine intermediates, or the alteration of physiological functions with the observed symptoms often remains very elusive, even unknown.

The adenylosuccinate lyase deficiency (OMIM 103050) is one of the most studied purine metabolism pathologies in which the functions of the Adsl enzyme, catalyzing two non-consecutive reactions required both for the salvage and *de novo* purine pathways, is altered (Figure 1A). First described in 1984 [9], this rare autosomal recessive disorder is associated with a massive accumulation in patient fluids (blood, urine and cerebrospinal fluid) of succinyl derivatives (Succinyl-adenosine and Succinyl-AICAR (AminoImidazole CarboxAmide

Ribonucleoside)) corresponding to dephosphorylation of the monophosphate substrates of Adsl (SZMP and SAMP, Figure 1A). The first patient-specific mutation in *ADSL* gene was identified in 1992 [10] and, to date, more than 50 different mutations have been described [11] (Figure S2, orange and yellow boxes). All the biochemically-studied mutations lead to a low residual Adsl enzymatic activity [12–16]. This pathology is characterized by serious neuro-muscular dysfunctions including psychomotor retardation, brain abnormalities, autistic features, seizures, ataxia, axial hypotonia, peripheral hypotonicity, muscular wasting and growth retardation [14,17,18]. Three distinct forms of *ADSL* deficiency have been categorized based on the severity of the symptoms: a fatal neonatal form (respiratory failure causing the death within the first weeks of life), a childhood form with severe neuromuscular symptoms (severe form; type I) and a more progressive form with milder symptoms (mild form; type II) (for review see [19]). A robust correlation has been clearly established between the residual activity of Adsl, the consequent accumulation of succinyl derivatives and the intensity of phenotypes [16,20–22]. However, these studies do not explain the molecular bases associated with *ADSL* deficiency, though they raise a real interest in identifying biological functions that could be modulated by SZMP, SAMP and their derivatives. For example, SZMP acts as a signal metabolite regulating transcriptional expression in yeast [8], it promotes proliferation in cancer cells by modulating pyruvate kinase activity [23] and SAMP stimulates insulin secretion in pancreatic cells [24]. More recently, RNA-seq analysis of a cellular model of *ADSL* deficiency identified misexpression of genes involved in cancer and embryogenesis, bringing some first clues to understanding the molecular bases of this rare disease [25].

To go further in the etiology of this disease, it is now essential to identify the different biological processes that are altered by a purine deficiency during embryonic development as the most severe symptoms appear *in utero* or within the first weeks or months after birth. To our knowledge, few invertebrate and vertebrate models have been developed to study this disease and no mammalian model recapitulating *ADSL* deficiency exists, most likely due to embryonic lethality [26,27]. Here, we establish a *X. laevis* model to assess the developmental functions of *ADSL* by knocking down its embryonic expression. This powerful vertebrate model organism has been widely used to identify developmental impairments associated with human pathologies [28,29].

We report the identification and functional validation of the *adsl.L* gene and show this gene as being mostly expressed in the nervous and muscular tissues during *X. laevis* development. Knock-down of *adsl.L* results in down-regulation at different developmental stages of several myogenic regulating factors (MRF), such as Myod1, Myf5 and Myogenin,

expression and leads to alterations in somites, craniofacial and hypaxial muscle formation, thus showing that *adsl.L* is essential for myogenesis. Finally, functional comparative analysis of other enzymes in the *de novo* and salvage purine pathways (Ppat.L, Ppat.S, and Hprt1.L) highlights a major role for purine metabolism in muscle tissue development, providing insight into the developmental defects that underlie some of the symptoms of patients with severe ADSL deficiency as well as other purine-associated pathologies.

2. Materials and Methods

2.1 Yeast media

SDcasaW is SD medium (0.5 % ammonium sulfate, 0.17 % yeast nitrogen base without amino acids and ammonium sulfate (BD- Difco; Franklin Lakes, NJ, USA) and 2 % glucose) supplemented with 0.2% casamino acids ((#A1404HA; Biokar/Solabia group; Pantin, France) and tryptophan (0.2 mM). When indicated, adenine (0.3 mM) or hypoxanthine (0.3 mM) was added as an external purine source in SDcasaW.

2.2 Yeast strains and plasmids

All yeast strains are listed in Table S1 and belong to, or are derived from, a set of disrupted strains isogenic to BY4741 or BY4742 purchased from Euroscarf (Germany). Double mutant strains were obtained by crossing, sporulation and micromanipulation of meiosis progeny. All plasmids (Table S2) were constructed using the pCM189 vector [30], allowing expression of *X. laevis* gene in yeast under the control of a tetracycline-repressible promoter. *X. laevis* open reading frame (ORF) sequences were amplified by PCR from I.M.A.G.E Clones (Source Biosciences; Nottingham, UK). All *X. laevis* ORF sequences were fully verified by sequencing after cloning in the pCM189 vector. Further cloning details are available upon request.

2.3 Yeast growth test

For drop tests, yeast transformants were pre-cultured overnight on solid SDcasaWA medium, re-suspended in sterile water at $1x10^7$ cells/ml and submitted to 1/10 serial dilutions. Drops (5 µl) of each dilution were spotted on freshly prepared SDcasaW medium plates supplemented or not with adenine or hypoxanthine. Plates were incubated either at 30 or 37 °C for 2 to 7 days before imaging.

2.4 Embryo culture

X. laevis males and females were purchased from the CNRS Xenopus Breeding Center (CRB, Rennes, France). Embryos were obtained by *in vitro* fertilization of oocytes collected in 1X Marc's Modified Ringers saline solution (1X MMR:100 mM NaCl, 2 mM KCl, 2 mM $CaCl_2$, 1 mM $MgSO_4$, 5 mM Hepes, pH 7.4), from a hormonally (hCG (Centravet), 450 units) stimulated female by adding crushed testis isolated from a sacrificed male. Fertilized eggs were de-jellied in 3% L-cysteine hydrochloride, pH 7.6 (Sigma-Aldrich), and washed several times with 0.1X MMR. Embryos were then cultured to the required stage in 0.1X MMR in the presence of 50 µM of gentamycin sulfate. Embryos were staged according to the Nieuwkoop and Faber table of *X. laevis* development [31].

2.5 mRNA synthesis and morpholino oligonucleotides

Capped mRNAs were synthesized using Sp6 mMESSAGE mMACHINE Kits (Ambion) from linearized plasmids (listed in Table S3). *Adsl.L*, *ppat.S*, *ppat.L* and *hprt1.L* RNA were transcribed from the IMAGE clones. *Adsl.L*-RNA*, *ppat.S*-RNA*, *ppat.L*-RNA* and *hprt1.L** ORFs were amplified by PCR in conditions which allow the introduction of mutations in the morpholino oligonucleotide (MO) binding site and were subcloned into the plasmid pBF. *Homo sapiens ADSL cDNA was subcloned into the plasmid pCS2+*. *Adsl.L* MO1 (5'-AAGCATGGAGGGGAGCAGTGGGCTAAG-3'), *Adsl.L* MO2 (5'-ATGGAGGGGAGCAGTGGGCTAAGCAT-3'), *hprt1.L* MO (5'-GGACACAGGCTCAGACATGGCGAGC-3'), *ppat.L*/*ppat.S* MO (5'-GTGATGGAGTTTGAGGAGCTGGGGAT-3') and standard control MO (cMO) were designed and supplied by Gene Tools, LLC. The position of the MOs in relation to their respective RNA is indicated in Figure S3.

2.6 Microinjections

Embryos were injected with MO alone or in combination with MO non-targeted mRNA (mutated *Adsl.L* RNA* or *Homo sapiens ADSL*, as specified in the text/legend) into the marginal zone of one blastomere at the 2-cell stage. *LacZ* (250 pg) RNA was co-injected as a lineage tracer. Embryos were injected in 5% Ficoll, 0.375X MMR, cultured to various developmental stages, fixed in MEMFA (MOPS 100 mM pH 7.4, EGTA 2 mM, $MgSO_4$ 1 mM, 4.0 % (v/v) formaldehyde) and stained for β-galactosidase activity using Red-Gal or X-Gal substrates (RES1364C-A103X or B4252, Merck) to identify the injected side and correctly targeted embryos. Embryos were fixed again in MEMFA before dehydration into 100% methanol or ethanol for immunohistochemistry or *in situ* hybridization, respectively.

2.7 In situ hybridization

Whole-mount *in situ* hybridizations (ISH) were carried out as previously described [32–34]. Sense and antisense riboprobes were designed by subcloning fragments of coding cDNA sequences in pBlueScript II (SK or KS) plasmids (Addgene). Riboprobes were generated by *in vitro* transcription using the SP6/T7 DIG RNA labelling kit (Roche, # 11175025910) after plasmid linearization as indicated in Table S4. Riboprobe hybridization detection was carried out with an anti-DIG Alkaline Phosphatase antibody (Roche, #11093274910) and the BM-Purple AP substrate (Roche, #11442074001). Riboprobes for *lbx1*, *mespa*, *myf5*, *myod1*, *myogenin*, *pax3*, *tbxt* (*xbra*) and *tcf15* were previously described [35–37].

2.8 Immunostaining

Whole-mount immunostaining of differentiated skeletal muscle cells was performed using the monoclonal hybridoma 12/101 primary antibody [38] (1/200 dilution; DSHB #AB-531892) and the EnVision^{+} Mouse HRP kit (Agilent Technologies, K4007) according to the manufacturer's recommendations.

2.9 Temporal expression of genes established by RT-PCR

RNA extraction from whole embryos, cDNA synthesis and RT-PCR were performed as previously described [33,39]. Sequences of the specific primers designed for each gene and PCR amplification conditions are given in Table S5. Chosen primers were selected to differentiate homeolog gene expression and to discriminate potential genomic amplification from cDNA amplification. PCR products were verified by sequencing (Eurofins genomics). The quantity of input cDNA was determined by normalization of the samples with the constant ornithine decarboxylase gene *odc1.L* [40]. Linearity of the signal was controlled by carrying out PCR reactions on doubling dilutions of cDNA and negative controls without either RNAs, reverse transcriptase and cDNA were also performed. Experiments were done at least twice on embryos from two different females ($N \geq 2$) and representative profiles are shown in Figure 2.

2.10 Embryo scoring and photography

Embryos were bleached (1% H_2O_2, 5% formamide, 0.5X SSC) to remove all visible pigment and phenotypes were determined in a commonly used way, blind-coded, by comparing the injected and un-injected sides. Only embryos with normal muscle tissue formation on the un-injected side and correctly targeted β-galactosidase staining on the injected side were scored.

Transverse sections were performed with a razor blade on fixed embryos. Embryos were photographed using a SMZ18 binocular system (Nikon).

2.11 Statistics and reproducibility

All experiments were carried out on at least two batches of fertilized eggs from two independent females ($N \geq 2$). Histograms represent the percentage of embryos displaying each phenotype and the number of embryos in each category is indicated in bars of each histogram. Fisher's exact test was used for statistical analyses and p-values are presented above the bars of the histogram in all figures.

2.12 Bioinformatics

Sequences were identified on the NCBI and Xenbase databases [41]. Basic Local Alignment Search Tool (BLAST) searches were performed on the NBCI Nucleotide and the Xenbase *X. laevis* 9.1 Scaffolds genome databases [42]. Conceptual translation of complementary DNA (cDNA) was performed on the ExPASy Internet website using the program Translate Tool (web.expasy.org/translate/). Comparison of coding sequences from *H. sapiens, S. cerevisiae, X. laevis* and *X. tropicalis* were done on https://blast.ncbi.nlm.nih.gov. Accession numbers of all sequences used in this study are given in Tables S6 and S7.

2.13 *Ethics statement*

All experimental procedures, performed in the Aquatic facility of the Centre Broca-Nouvelle Aquitaine in Bordeaux EU0655, complied with the official European guidelines for the care and use of laboratory animals (Directive 2010/63/EU) and were approved by the Bordeaux Ethics Committee (CEEA50) and the French Ministry of Agriculture (agreement #A33 063 942, approved 2018/07/27).

3. Results

3.1 Identification of X. laevis purine pathway genes

The purine biosynthesis pathways are known to be highly conserved throughout evolution [1]. Most of *X. laevis* genes encoding potential purine-pathway enzymes have been putatively identified and annotated by automated computational analyses from the entire genome sequencing [43]. Protein sequences were deduced from conceptual translation of these annotated genes and aligned with their potential orthologs, e.g. *H. sapiens* and *X. tropicalis*

(Table S6). The vast majority of *X. laevis de novo* and salvage pathways have two homeologs, whose protein sequences display a high degree of identity with their *X. tropicalis* and human orthologs (more than 85 and 50 %, respectively ; Figure 1A and Table S6), suggesting that these annotated genes effectively encode the predicted purine-pathway enzymes.

To establish that the putative *X. laevis* purine-pathway genes encode the predicted enzymatic activities, a functional complementation assay was undertaken by heterologous expression of *X. laevis* genes in the yeast *Saccharomyces cerevisiae,* which has been proven to be a valuable model to investigate metabolic pathways [44]. Yeast knock-out mutants were available in the laboratory and sequence alignments showed a high degree of identity between *S. cerevisiae* and *X. laevis* orthologous protein sequences (Figure S1 and Table S7). Plasmids-allowing expression of the *X. laevis* ORF in *S. cerevisiae* were transformed in the cognate yeast knock-out mutant, and functional complementation was tested. As shown in Figure 1B, the yeast *adsl* knock-out mutant (*ade13*) was unable to grow in the presence of hypoxanthine as a unique purine source, but growth was restored by the expression of either the *S. cerevisiae ADE13* or the *X. laevis adsl.L* gene. By contrast, all these strains were able to grow in the presence of adenine that allow purine synthesis *via* the adenine phosphoribosyl transferase (Apt1) and AMP deaminase (Amd1) activities (Figure S1). Similar experiments were conducted with 15 other *X. laevis* purine-pathway encoding genes, 13 of which were able to complement the *S. cerevisiae* cognate knock-out mutants (Figure S4 and Figure S5). Altogether, this data allowed us to functionally validate *adsl.L* and 13 other *X. laevis* genes involved in purine *de novo* and recycling pathways, demonstrating that the purine pathways are functionally conserved in *X. laevis*.

We then focused on the role of adenylosuccinate lyase as: (1) it is encoded by a single gene (*adsl.L),* greatly simplifying knock-down experiments, and its protein sequence is highly conserved between human and *X. laevis* (Figure S2), (2) it is the only enzymatic activity that is required in both the *de novo* biosynthesis and recycling purine pathways, and (3) its mutation leads to severe developmental alterations, for which the molecular bases associated with the symptoms are still largely unknown.

3.2 The adsl.L gene is mostly expressed in muscular and neuronal tissues and their precursors during X. laevis development.

Adsl.L spatiotemporal expression during *X. laevis* development was established by two complementary approaches. First, its temporal expression profile was determined by RT-PCR

on whole embryos from fertilized egg to stage 45 (Figure 2A). The *adsl.L* gene displays both a maternal (before the mid-blastula transition (MBT)) and a zygotic expression at all developmental stages studied.

Adsl.L spatial expression was then determined by *in situ* hybridization (Figure 2B). *Adsl.L* expression is detected in the animal, but not vegetal, pole during the cleavage phase. Zygotic expression was detected in the neuroectoderm and in the paraxial mesoderm during neurulation. From stage 25 until the late organogenesis stages, *Adsl.L* expression was found in the developing epibranchial placodes, lens and in the central nervous system (fore-midbrain and mid-hindbrain boundaries). From stage 30 onwards, *Adsl.L* transcripts were also detected in the somites and its somitic expression appeared to increase during organogenesis. At the late organogenesis stage, its expression was detected in other mesoderm-derived tissues, such as the pronephric tubules (proximal and intermediate tubules) and the heart.

Using similar approaches, we showed that (1) 14 out of the 16 tested genes display a similar temporal expression profile to that of *adsl.L* (Figure S6) and (2) all 9 genes tested by *in situ* hybridization are expressed in neuro-muscular tissues (e.g. somites, hypaxial muscles, central nervous system and retinas), even if differences in the tissue specificity exist for some of these genes (Figures S7-S8). These spatio-temporal expression patterns are consistent with the fact that neuromuscular dysfunctions are the primary symptoms associated with purine-dependent diseases.

3.3 The adsl.L gene is required for X. laevis myogenesis

To understand the role of *Adsl.L* during muscle development, we have undertaken a loss of function approach using two specific anti-sense morpholino oligonucleotides (MOs) (see Figure S3A for MOs efficiency). MOs injections were performed in the marginal zone of one blastomere at the 2-cell stage. This injection has the advantage of unilaterally affecting the development of the future mesoderm, with the non-injected side serving as an internal control. A dose-dependent curvature along the anterior/posterior axis was observed following injection of *adsl.L* MO1 and MO2, and not of the control morpholino (cMO), with a concave deformation always corresponding to the side of injection (Figure 3A-B). This curvature phenotype was already documented when myogenesis was altered [45], suggesting that *adsl.L* gene could be required for proper muscle formation in *X. laevis*. To test this hypothesis, we performed immunostaining on tailbud and tadpole stages with the differentiated skeletal muscle cells-specific 12-101 antibody [38]. cMO injected embryos displayed normal global morphology and

normal muscle phenotype at all stages tested. By contrast, myotomes were smaller along the dorsoventral axis following the injection of 10 ng of *adsl.L* MO1 or MO2 at the tailbud stage (Figure 3 C-D). Furthermore, somite morphology was considerably altered. Straight-shape somites, blurred somite domains and fewer v-shape somites were observed on the injected side. 12-101 positive area was also reduced along the anteroposterior axis, the latter shortening most likely being at the origin of the curvature phenotype observed (Figure 3A). This muscle alteration was even more exacerbated by increasing the dose of MO, with severe reduction and in some cases, absence of 12/101 positive domain and no somitic-like structure observed on the injected side in more than 80% of the injected 20 ng MO1 embryos (Figure 3C). This dose-dependent muscle phenotype was still observed in the tadpole stage (stage 39) with a similar percentage of *Adsl.L* morphant embryos displaying myotome reduction and altered chevron-shaped somites in their injected side, especially in the anterior trunk region (Figure S9A-B). At the late tadpole stage (stage 41), somite defects, characterized by anterior straight or criss-crossed somites, were observed on the injected side of *adsl.L* morphants (red arrowheads; Figure 3E-F), whereas the cMO embryo injected side displayed the characteristic v-shaped somites (white arrowheads; Figure 3E-F). Reduction of the hypaxial muscles (precursors of the limb muscles) was also observed in *adsl.L* morphants but not in cMO injected embryos (Figure 3E, G, compare the blue to the white dashed areas in *adsl.L* MO1 embryo). This hypaxial muscle phenotype was worsened when the MO dose was increased with no hypaxial muscle progenitors in 70% and 96% of analyzed embryos following 10 ng and 20 ng of *Adsl.L* MO1 injection respectively (Figure S9A, C). These phenotypes were rescued by co-injecting *adsl.L* MO1 with the *adsl.L* mutated RNA*, whose translation is unaffected (Figure S3A) by *adsl.L* MO1 and MO2 (Figure 3E-G). No significant phenotype was obtained by co-injecting the *adsl.L* RNA* with cMO (Figure 3E-G). Together, these results validate the muscular-associated phenotypes as a consequence of a specific *adsl.L* gene knock-down and not of the potential morpholino injection's side effects.

To confirm *adsl.L* gene implications during myogenesis, expression of *tcf15* (*paraxis*) and *mespa* (*thylacine* 1) genes was analyzed in *adsl.L* MO1 and MO2 morphants at late neurula stages (stages 17-19). As expected, *tcf15* expression was observed in the dorsolateral part of the somites [35] following control cMO injection. However, its expression domain was reduced following *adsl.L* knock-down (Figure 4A-B), suggesting that the primitive myotome formation is impacted in *adsl.L* morphants. Alterations in expression of *mespa*, a somitomere marker [46,47], were also observed in *adsl.L* knock-down conditions (Figure 4C, D). These alterations included reduction, even an absence, of mespa stripes number and of their lateral length. The

most frequent phenotype was a shift to a more anterior position in the presomitic mesoderm (white arrows, Figure 4C). These significant phenotypes suggest that *adsl.L* is involved in the segmentation of the presomitic mesoderm.

To determine whether the observed muscle phenotypes were specifically related to the knock-down of the *adsl.L* gene or to the purine pathways alteration, similar loss of function experiments (see Figure S3B-C for MOs efficiency) were carried out on other purine-associated genes: (1) the *ppat* (*ppat.L* and *ppat.S*) genes encoding the phosphoribosylpyrophosphate amidotransferase (Ppat), the first enzyme of the purine *de novo* pathway, and (2) the *hprt1.L* gene encoding the Hypoxanthine-PhosphoRybosylTransferase (Hprt) in the salvage pathway (Figure 1A), the enzyme allowing metabolization of hypoxanthine, the major purine source in *X. laevis* embryos [48]. Comparable muscle alterations were obtained with independent knock-down of these genes, *i.e.* a strong alteration of somite shape at both the tailbud and tadpole stages, associated with smaller myotomes at the early organogenesis stage and reduction, or even absence, of hypaxial muscles in the latter stages (Figure S10 and S11). Myogenesis alterations were also observed at neurula stages (Figures S12 and S13). Reduction of *tcf15* expression domain was observed following *ppat* and *hprt1.L* MO injection (Figure S12). Furthermore, formation of somitomeres was disrupted in *ppat* and *hprt1.L* morphants, which showed a shift and number reduction of mespa stripes on the injected side (Figure S13).

Taken together, these similar muscle phenotypes observed in *adsl.L*, *ppat* and *hrpt1.L* morphants demonstrate a strong association between altered purine pathways and defects in somitogenesis and myogenesis.

3.4 Expression of the myod1 and myf5 genes requires functional purine pathways

We assessed whether the muscular phenotypes observed upon knock-down of purine-associated genes could result from an alteration of the myogenic regulatory factor's (MRFs) expression during the different myogenic waves [36,49]. Expression of both *myod1* and *myf5* was first analyzed by *in situ* hybridization at the early neurula stage, during the first myogenic wave (Figure 5 A-D). A strong reduction of both *myod1* and *myf5* expression was observed on the injected side of *adsl.L* morphants (Figure 5 A, C), whereas no alteration could be seen in cMO-injected embryos. This significant reduction was even stronger in the anterior region, which will give rise to the first somites. Importantly, *myod1* expression was rescued by the injection of *X. laevis adsl.L* mutated RNA* or human *ADSL* RNA in *adsl.L* MO1 and MO2 morphants (Figure 5A-B). These results are consistent with an adenylosuccinate lyase activity, even heterologous, being required for the proper expression of *myod1*. Of note, over-expression

of either *X. laevis adsl.L* mutated RNA* or human *ADSL* mRNA induced a small but significant increase in *myod1* expression (Figure S14). To exclude that the observed reduction of *myod1* and *myf5* expression resulted from an alteration of mesoderm formation and/or integrity in *adsl.L* morphants, expression of the pan-mesoderm marker *tbxt* (*xbra*) was analyzed by *in situ* hybridization on whole embryos at stage 11. No significant difference was observed in all injected embryos (Figure 5E). Finally, a strong and similar reduction in *myod1* expression, with no alteration of the *tbxt* gene expression pattern, was also observed in either *ppat.L/ppat.S* or *hprt1.L* morphants (Figure S15). Altogether, these results show that functional purine synthesis is strictly required for a proper expression of the myogenic regulatory factor genes *myod1* and *myf5* during the first myogenic wave.

To further analyze the effects of *adsl.L* knock-down on MRF expression, *myod1* and *myf5* expression was then analyzed at later developmental stages (Figure 6). At the tailbud stage, the *myod1* expression in the somites was found markedly altered in *adsl.L* MO1 and MO2 morphants. As observed with the 12/101 staining, myotomes were shortened along the dorsoventral axis and somite shape defects, and even loss of the chevron V-shape of the most anterior somites, were observed (blue arrowheads, Fig 6 A-B). *Myod1* expression in the ventral border of the dermomyotome was also markedly reduced or lost (red arrowheads, Fig 6 A-B), while its expression in the dermomyotome dorsal border was less altered in the anterior trunk region. Expression of *myod1* in craniofacial muscles was also reduced, or even absent following *adsl.L* MO1 or MO2 injection (green arrowheads, Fig 6 A-B). These alterations in craniofacial muscles were also observed at the tadpole stages with a severe significant reduction of *myod1* expression especially in the interhyoideus (ih), quadrato-hyoangularis and orbitohyoideus anlagen (q/oh), in *adsl.L* MO1 and MO2 morphants (light green arrowheads, Fig 6C-D). Expression of *myf5* was also noticeably altered in craniofacial muscles at both the tailbud and tadpole stages (Figure 6E-H), even if these alterations are milder than the *myod1* ones. Indeed, *myf5* expression in *adsl.L* morphants is reduced or absent at both stages in the dorsal region of the pharyngeal arch muscle anlagen (black arrowhead, Figure 6G), whereas its expression in the interhyoideus and the intermandibularis muscle anlagen is rarely reduced (pink arrowhead, Figure 6G). However, no alteration of *myf5* expression was observed in the undifferentiated pre-somitic mesoderm in the tail region (yellow circles, Figure 6E-H). The implication of *adsl.L* in the formation of the cranial muscles was also confirmed by analyzing the expression of myogenin (*myog*) following *adsl.L* MO1 and MO2 injection at stage 39 (Figure 7A and Figure S16). A strong reduction, even an absence, of *myogenin* staining in the pharyngeal arch muscle anlagen was observed on the injected side in *adsl.L* morphants, whereas its expression in the

interhyoideus and intermandibularis muscle anlagen was, however, less affected. These results are consistent with those observed by 12-101 immunolabelling on *adsl.L* morphants (Figure S9, blue arrowhead). Altogether, these data show that *adsl.L* is required for *myod1*, *myf5* and *myogenin* expression during the second wave of myogenesis.

3.5 The adsl.L gene is required for hypaxial muscle formation and migration

In addition to the somite and craniofacial muscle phenotypes, severe hypaxial muscle alterations were observed in *adsl.L* morphants (Figure 3 and Figure S9). To further characterize these defects, the expression of *myogenin* was analyzed by *in situ* hybridization at the late tadpole stage. *Adsl.L* knock-down resulted in either a strong decrease or even an absence of *myog* expression in hypaxial muscle cells, while no significant alteration was observed in the embryos injected with the control morpholino (cMO) in combination or not with the *adsl.L* mutated RNA* (Figure 7A-B). This muscle phenotype was rescued by the injection of the *adsl.L* mutated RNA* in *adsl.L* MO2 morphants. These *myogenin* expression alterations were confirmed as *myod1* expression is strongly reduced or absent in hypaxial muscles in *adsl.L* morphants (purple arrowheads, Figure 6C and Figure S17). These results confirm the role of the *adsl.L* gene in the expression of myogenic regulatory factors required for correct hypaxial muscle development. In addition, hypaxial muscles were also found to be highly reduced or absent as revealed by 12-101 immunolabelling in *ppat.L/ppat.S* and *hprt1.L* morphants (pink arrowheads, Figure S10-S11). Interestingly, hypaxial muscle defects have also been observed in *tcf15* knock-out mice [50], a gene whose expression is altered in purine *X. laevis* morphants (Figure 4A).

To better understand the deleterious effect of *adsl.L* knock-down on hypaxial muscles, expression of the *pax3* and *lbx1* genes encoding transcription factors were analyzed at tadpole stages. *Lbx1* and *pax3* are both expressed in hypaxial body wall undifferentiated cells that form the front of hypaxial myoblast migration [37,51]. Although the injection of *adsl.L* MO, especially *adsl.L* MO2, induces a slight reduction of *lbx1* expression in the hypaxial muscle precursors, the major observed phenotype is a migration alteration of these *lbx1* positive cells (Figure 7C-D). Indeed, muscle progenitors are closer to the ventral border of the somites. This alteration is more pronounced in the most anterior region (trunk I), in which progenitors migrate around the hyoid region (see yellow double arrows in Figure 7C). Similar alterations were observed for *pax3* positive hypaxial body wall progenitors, characterized by a severe alteration of hypaxial progenitor migration, while *pax3* expression is less or not affected in the hypaxial

myotome (Figure 7E-F). Altogether, these results show that purine biosynthesis genes are essential during hypaxial muscle formation in *X. laevis*.

4. Discussion

4.1 X. laevis as a vertebrate model to study purine deficiency related pathologies

In this study, we functionally characterized for the first time the main members of the purine biosynthesis and salvage pathways in the vertebrate *X. laevis*. We also established the comparative map of their embryonic spatiotemporal expression and showed that the main common expression of purine genes is in the neuro-muscular tissue and its precursors. This expression profile can be directly linked to the neuro-muscular symptoms usually observed in most of the nearly thirty identified purine-associated pathologies [3–7]. Furthermore, we investigated the embryonic roles of three purine biosynthesis enzymes during vertebrate muscle development, focusing on the Adsl.L enzyme. As *ADSL* deficiency in humans is associated with a residual enzymatic activity (reviewed in [6,52]), we believe that our experimental strategy based on the knockdown with morpholino-oligonucleotides is more appropriate in identifying the molecular dysfunctions found in patients rather than strategies based on knock-out experiments. Altogether, our data shows that *X. laevis* is a relevant model in studying the molecular bases of the developmental alterations associated with purine deficiencies.

4.2 Role of purine pathway genes during X. laevis development

Maternal and zygotic expression are key indicators of potential pathway involvement during vertebrate development. We show that the early stages of *X. laevis* embryo development is dependent on both purine pathways, as all the genes studied, except for *adss1.L* and *adss1.S*, are maternal genes and are expressed from gastrula stages. However, from the early organogenesis phase (stage 22), all the 17 tested genes are expressed. We have previously shown that the unique reserve of purine in embryos, hypoxanthine, is depleted at stage 22 [48], so this embryonic stage is placed as a key turning point of purine source for the embryo. From this stage onwards and until stage 45 (stage where embryos start to feed), purines can only be synthesized *de novo* or recycled within the embryo, and zygotic expression of purine biosynthesis genes becomes then crucial.

Furthermore, the genes of the purine *de novo* and salvage pathways share simultaneous embryonic expression and mostly in the same tissues, strongly suggesting that neither pathway is preferred for purine supply during *X. laevis* development. Our functional experiments also

demonstrate that both pathways are involved in development since the muscle alterations observed in *adsl.L* morphants were also observed in *ppat.L/ppat.S* and *hprt1.L* morphants. This is different from what has been obtained in *C. elegans* in which muscle phenotypes associated with *ADSL* deficiency are rather dependent on the purine recycling pathway [27].

In addition, we have shown that *adsl.L* plays an early and essential role in myogenesis, during the first and second myogenic wave, and its knock-down is associated with strong alterations in primary myotome, somitomeres and anterior somite formation and subsequent malformation of hypaxial and craniofacial muscles. Embryonic neuro-muscular defects have previously been described in other animal models [26,27], with a strong alteration in muscle integrity observed in *C. elegans adsl* knockout mutants. These studies raised the question of whether the observed phenotypes were the result of a decrease in one or more end products of the purine biosynthetic pathways, or that of an accumulation of Adsl.L substrates or their derivatives. Indeed, the neurodevelopmental alterations observed in zebrafish *adsl* mutants were associated with the accumulation of SAICAr, the dephosphorylated form of Adsl substrate in the *de novo* pathway (SAICAR, or SZMP) and thus these neuronal alterations were rescued by inhibition of this pathway [26]. In *X. laevis*, as the alterations in myogenesis are very similar in the *adsl.L*, *ppat.L*/*ppat.S* and *hprt1.L* morphants, it seems very unlikely that the muscle phenotypes are related to an accumulation of Adsl.L substrates or their derivatives (Figure 1A). A metabolic rescue of the phenotypes is, therefore, an appropriate strategy to determine whether the muscle phenotypes could be related to a decrease in Adsl.L products and/or downstream metabolites. Hypoxanthine, the main source of purine in *X. laevis* embryo [48], would have been the best candidate metabolite for the MO rescue but it cannot be tested here since its metabolization requires the enzymatic activity of Adsl.L (Figure 1A). Rescue experiments were therefore carried out by adding adenine to the *adsl*.L morphant culture medium in concentrations at which this purine precursor was soluble in the medium (50 µM) but without any success. We cannot rule out that this may be due to the incapacity of this purine to cross the vitelline membrane. However, rescue experiments by adenine injection into the blastocoel or archenteron, as previously performed for other purine [32,53], is not possible because of its low solubility in aqueous solutions (< few µM).

Overall, these results strongly suggest that the observed muscle phenotypes are associated with purine deficiency, regardless of the mode of biosynthesis of these purines, since disruption of the *de novo* pathway (*ppat.L*/*ppat.S* MO), the recycling pathway (*hprt1.L* MO), or both (*adsl.L* MO) results in similar alterations in myogenesis. However, these alterations

may explain the muscle symptoms such as axial hypotonia, peripheral hypotonia and muscle wasting observed in patients [14,17,18].

4.3 Muscle defects associated with purine pathways dysfunction are related to an altered expression of MRF genes

Our study provides new *in vivo* evidence for the identification of altered molecular mechanisms during purine deficiency. Indeed, we show that functional purine pathways are required for the expression of the myogenic regulator factors MyoD1, Myf5 and Myogenin, which are by far the master regulatory transcription factors of the embryonic myogenic program including myotome and somite formation, hypaxial and craniofacial myogenesis [36,49]. The *adsl.L*-specific alteration of *myod1* and *myf5* expression in the ventral border of the dermomyotome could, therefore, be at the origin of the deleterious effects observed in morphants on hypaxial progenitors and differentiated hypaxial muscle cells. A strong decrease in MRF expression was observed in *adsl.L* morphants from the earliest stages of muscle formation in neurula embryos. As MRF genes regulate the expression of other MRFs and/or their own expression, it is possible that one (or more) key purine derivative(s) could regulate the transcription expression and/or the function of one of the MRF. Interestingly, the opposite phenotypes were obtained on *myod1* expression in *adsl.L* morphants and in embryos overexpressing this gene, placing *adsl.L* as a key regulator of *myod1* expression during development. Since MyoD1 is a potent inducer of muscle differentiation and is required for *myf5* expression in early *X. laevis* development, correct anterior somite segmentation [54] and for correct myotome size [35], it is, therefore, possible that the muscle defects in *adsl.L* morphants are mainly due to a deregulation of *myod1* expression, thus placing this gene, and the purine biosynthetic pathways, at the top of the myogenic gene cascade. An interesting future point of investigation would be to test whether Myod1 expression is able to rescue adsl morphant muscle phenotypes.

So far, we have not found a direct nor an indirect link between purines and the transcriptional regulation of MRFs. However, regulation of transcription factor activity by direct binding of purine metabolites has already been demonstrated in different organisms [8,55]. In yeast, we have shown that the direct binding of purine metabolites (SZMP and ZMP, Figure 1) on Pho4 and Pho2 transcription factors was responsible for their activation [8]. These two metabolites of the *de novo* purine pathway are certainly not those implicated here as similar muscle phenotypes were obtained in *adsl.L*, *ppat.L*/*ppat.S* and *hprt1.L* morphants, but we can speculate that another purine derivative could similarly be involved in modulating the

transcriptional expression of MRFs during *X. laevis* myogenesis. Moreover, regulation of *myogenin* gene expression by metabolites (CMP and UMP) has recently been observed in the mouse C2C12 cell line [56], showing that MRF expression can be modulated by nucleotides. To our knowledge, a similar direct regulation of MRFs by purines has not been described to date. If it exists, as suggested by our data, then the mechanism by which it acts remains to be established.

It may be possible that the effect of purines on MRFs expression is indirect via upstream cascades, responding to purines, and regulating the expression of these genes. Indeed, many upstream signals, for example, Wnt and FGF, regulate the expression of MRFs in myogenesis (reviewed in [57]). These pathways involve the activation of protein kinases of the myogenic kinome whose activity is highly dependent on intracellular pools of purine nucleotides [58]. In particular, the activity of protein kinase A, initiated by the activation of heteromeric G proteins and adenylate cyclase through the Wnt pathway, is required for the expression of *myod1* and *myf5* and the formation of myoblasts. In addition, extracellular triphosphate purine nucleotides are ligands of purinergic receptors which are involved in myoblast proliferation and differentiation [59,60]. We have recently shown that the ATP-dependent P2X5 receptor subunit is specifically expressed in *X. laevis* somites, which is in agreement with its expression profile described in other animal models [61,62]. We may hypothesize that *adsl.L* knock-down may reduce the availability of extracellular purines, leading to a possible alteration in P2X5 activation and myogenesis impairment [62]. This hypothesis will be tested in the next future in the laboratory. We had previously shown that purinergic signaling controls vertebrate eye development by acting on the expression of the PSED (*pax*/*six*/*eya*/*dach*) network genes [29]. As this PSED gene network regulates MRF expression [63], it may be also possible that a similar mechanism is involved in *adsl.L* morphants. Interestingly, our observed muscle phenotypes are highly similar to those induced by retinoic acid receptor β2 (RARβ2) loss of function, *i.e.* a rostral shift of presomitic markers, defects in somite morphology, chevron-shaped somites, and hypaxial muscle formation [64]. Retinoic acid pathway, through the activation of RAR, regulates myogenic differentiation and MRF gene expression [65]. It has been reported that retinoic acid affects synthesis of PRPP in human erythrocytes in Psoriasis [66] and RA deficiency interferes with the expression of genes involved in the purine metabolism pathway *in vivo* [67]. These data along with ours suggest a possible link between purine biosynthetic pathway, retinoic acid signaling pathway and MRF gene expression, worth of further studies in the future.

In conclusion, the establishment of this new animal model allowed us to demonstrate the critical functions of the purine biosynthetic pathways during vertebrate embryogenesis. Indeed, our results provide evidence for the roles for purine pathway genes in myogenesis through the regulation of MRF gene expression during embryogenesis. Although the first median and lateral myogenesis disappeared during evolution, the second myogenic wave is conserved [49]. We can, therefore, speculate that the involvement of the *de novo* and salvage purine pathways during this myogenic wave is conserved in mammals and that purines may, therefore, be key regulators in the formation of hypaxial myogenic cells, the progenitors of the abdominal, spinal, and limb muscles, those muscles which are affected in patients with purine-associated pathologies [4,5,7,52]. Although, in this work we have mostly focused on muscle alterations, it provides the basis for further functional studies to identify the molecular mechanisms involved in the development of neuromuscular tissues, those tissues in which the alterations underlie the major deleterious symptoms of patients with purine deficiency.

Author contributions: Conceptualization, B.P. and K.M.; methodology, B.P., C.S-M, E.H., F. H, K.M. and M.D.; Formal analysis, B.P., K.M. and M.D.; Investigation, B.P., C.S-M, E.H., F. H, K.M. and M.D..; Resources, B.D-F, B.P., C.S-M, E. B-G., E.H., F. H, K.M. and M.D.; Writing-original draft preparation, B.P., K.M.; Supervision, B.P. and K.M. All authors have read and agreed to the published version of the manuscript.

Fundings: This work was supported by recurrent funding from the Centre National de la Recherche Scientifique (CNRS), and from PEPS/IDEX CNRS/Bordeaux University and the "Association Retina France" to B.P.

Acknowledgments: The author thanks C. Blanchard, A. Martinez and A. Tocco for their technical help, D. Patterson for generous gift of the pADSLpCR3.1 plasmid used to clone human *ADSL*-pCS2+ plasmid for the rescue experiments, C. Chanoine and B. Della Gaspera for generous gift of the plasmids used for *mespa*, *myogenin* and *tcf15 in situ* hybridization probes, J.E. Gomes for critical reading of the manuscript, and K. Chiimba and S. Sanghera for English proofreading.

Conflicts of interest: The authors declare no conflict of interest.

References

1. Daignan-Fornier, B.; Pinson, B. Yeast to Study Human Purine Metabolism Diseases. *Cells* **2019**, *8*, E67, doi:10.3390/cells8010067.
2. Massé, K.; Dale, N. Purines as Potential Morphogens during Embryonic Development. *Purinergic Signal.* **2012**, *8*, 503–521, doi:10.1007/s11302-012-9290-y.
3. Simmonds, H.A.; Duley, J.A.; Fairbanks, L.D.; McBride, M.B. When to Investigate for Purine and Pyrimidine Disorders. Introduction and Review of Clinical and Laboratory Indications. *J. Inherit. Metab. Dis.* **1997**, *20*, 214–226, doi:10.1023/a:1005308923168.
4. Balasubramaniam, S.; Duley, J.A.; Christodoulou, J. Inborn Errors of Purine Metabolism: Clinical Update and Therapies. *J. Inherit. Metab. Dis.* **2014**, *37*, 669–686, doi:10.1007/s10545-014-9731-6.
5. Jurecka, A. Inborn Errors of Purine and Pyrimidine Metabolism. *J. Inherit. Metab. Dis.* **2009**, *32*, 247–263, doi:10.1007/s10545-009-1094-z.
6. Nyhan, W.L. Disorders of Purine and Pyrimidine Metabolism. *Mol. Genet. Metab.* **2005**, *86*, 25–33, doi:10.1016/j.ymgme.2005.07.027.
7. van den Berghe, G.; Vincent, M.-F.; Marie, S. Disorders of Purine and Pyrimidine Metabolism. In *Inborn Metabolic Diseases: Diagnosis and Treatment*; Fernandes, J., Saudubray, J.-M., van den Berghe, G., Walter, J.H., Eds.; Springer: Berlin, Heidelberg, 2006; pp. 433–449 ISBN 978-3-540-28785-8.
8. Pinson, B.; Vaur, S.; Sagot, I.; Coulpier, F.; Lemoine, S.; Daignan-Fornier, B. Metabolic Intermediates Selectively Stimulate Transcription Factor Interaction and Modulate Phosphate and Purine Pathways. *Genes Dev.* **2009**, *23*, 1399–1407, doi:10.1101/gad.521809.
9. Jaeken, J.; Van den Berghe, G. An Infantile Autistic Syndrome Characterised by the Presence of Succinylpurines in Body Fluids. *Lancet Lond. Engl.* **1984**, *2*, 1058–1061.
10. Stone, R.L.; Aimi, J.; Barshop, B.A.; Jaeken, J.; Van den Berghe, G.; Zalkin, H.; Dixon, J.E. A Mutation in Adenylosuccinate Lyase Associated with Mental Retardation and Autistic Features. *Nat. Genet.* **1992**, *1*, 59–63, doi:10.1038/ng0492-59.
11. Mao, X.; Li, K.; Tang, B.; Luo, Y.; Ding, D.; Zhao, Y.; Wang, C.; Zhou, X.; Liu, Z.; Zhang, Y.; et al. Novel Mutations in ADSL for Adenylosuccinate Lyase Deficiency Identified by the Combination of Trio-WES and Constantly Updated Guidelines. *Sci. Rep.* **2017**, *7*, 1625, doi:10.1038/s41598-017-01637-z.
12. Van den Bergh, F.; Vincent, M.F.; Jaeken, J.; Van den Berghe, G. Residual Adenylosuccinase Activities in Fibroblasts of Adenylosuccinase-Deficient Children: Parallel Deficiency with Adenylosuccinate and Succinyl-AICAR in Profoundly Retarded Patients and Non-Parallel Deficiency in a Mildly Retarded Girl. *J. Inherit. Metab. Dis.* **1993**, *16*, 415–424, doi:10.1007/BF00710291.
13. Kmoch, S.; Hartmannová, H.; Stibůrková, B.; Krijt, J.; Zikánová, M.; Sebesta, I. Human Adenylosuccinate Lyase (ADSL), Cloning and Characterization of Full-Length cDNA and Its Isoform, Gene Structure and Molecular Basis for ADSL Deficiency in Six Patients. *Hum. Mol. Genet.* **2000**, *9*, 1501–1513, doi:10.1093/hmg/9.10.1501.
14. Mouchegh, K.; Zikánová, M.; Hoffmann, G.F.; Kretzschmar, B.; Kühn, T.; Mildenberger, E.; Stoltenburg-Didinger, G.; Krijt, J.; Dvoráková, L.; Honzík, T.; et al. Lethal Fetal and Early Neonatal Presentation of Adenylosuccinate Lyase Deficiency: Observation of 6 Patients in 4 Families. *J. Pediatr.* **2007**, *150*, 57-61.e2, doi:10.1016/j.jpeds.2006.09.027.
15. Jurecka, A.; Zikanova, M.; Tylki-Szymanska, A.; Krijt, J.; Bogdanska, A.; Gradowska, W.; Mullerova, K.; Sykut-Cegielska, J.; Kmoch, S.; Pronicka, E. Clinical, Biochemical and Molecular Findings in Seven Polish Patients with Adenylosuccinate Lyase Deficiency. *Mol. Genet. Metab.* **2008**, *94*, 435–442, doi:10.1016/j.ymgme.2008.04.013.

16. Zikanova, M.; Skopova, V.; Hnizda, A.; Krijt, J.; Kmoch, S. Biochemical and Structural Analysis of 14 Mutant Adsl Enzyme Complexes and Correlation to Phenotypic Heterogeneity of Adenylosuccinate Lyase Deficiency. *Hum. Mutat.* **2010**, *31*, 445–455, doi:10.1002/humu.21212.
17. Spiegel, E.K.; Colman, R.F.; Patterson, D. Adenylosuccinate Lyase Deficiency. *Mol. Genet. Metab.* **2006**, *89*, 19–31, doi:10.1016/j.ymgme.2006.04.018.
18. Gitiaux, C.; Ceballos-Picot, I.; Marie, S.; Valayannopoulos, V.; Rio, M.; Verrieres, S.; Benoist, J.F.; Vincent, M.F.; Desguerre, I.; Bahi-Buisson, N. Misleading Behavioural Phenotype with Adenylosuccinate Lyase Deficiency. *Eur. J. Hum. Genet. EJHG* **2009**, *17*, 133–136, doi:10.1038/ejhg.2008.174.
19. Jurecka, A.; Zikanova, M.; Kmoch, S.; Tylki-Szymańska, A. Adenylosuccinate Lyase Deficiency. *J. Inherit. Metab. Dis.* **2015**, *38*, 231–242, doi:10.1007/s10545-014-9755-y.
20. Marie, S.; Race, V.; Vincent, M.F.; Van den Berghe, G. Adenylosuccinate Lyase Deficiency: From the Clinics to Molecular Biology. *Adv. Exp. Med. Biol.* **2000**, *486*, 79–82, doi:10.1007/0-306-46843-3_15.
21. Race, V.; Marie, S.; Vincent, M.F.; Van den Berghe, G. Clinical, Biochemical and Molecular Genetic Correlations in Adenylosuccinate Lyase Deficiency. *Hum. Mol. Genet.* **2000**, *9*, 2159–2165, doi:10.1093/hmg/9.14.2159.
22. Mastrogiorgio, G.; Macchiaiolo, M.; Buonuomo, P.S.; Bellacchio, E.; Bordi, M.; Vecchio, D.; Brown, K.P.; Watson, N.K.; Contardi, B.; Cecconi, F.; et al. Clinical and Molecular Characterization of Patients with Adenylosuccinate Lyase Deficiency. *Orphanet J. Rare Dis.* **2021**, *16*, 112, doi:10.1186/s13023-021-01731-6.
23. Keller, K.E.; Tan, I.S.; Lee, Y.-S. SAICAR Stimulates Pyruvate Kinase Isoform M2 and Promotes Cancer Cell Survival in Glucose-Limited Conditions. *Science* **2012**, *338*, 1069–1072, doi:10.1126/science.1224409.
24. Gooding, J.R.; Jensen, M.V.; Dai, X.; Wenner, B.R.; Lu, D.; Arumugam, R.; Ferdaoussi, M.; MacDonald, P.E.; Newgard, C.B. Adenylosuccinate Is an Insulin Secretagogue Derived from Glucose-Induced Purine Metabolism. *Cell Rep.* **2015**, *13*, 157–167, doi:10.1016/j.celrep.2015.08.072.
25. Mazzarino, R.C.; Baresova, V.; Zikánová, M.; Duval, N.; Wilkinson, T.G.; Patterson, D.; Vacano, G.N. The CRISPR-Cas9 crADSL HeLa Transcriptome: A First Step in Establishing a Model for ADSL Deficiency and SAICAR Accumulation. *Mol. Genet. Metab. Rep.* **2019**, *21*, 100512, doi:10.1016/j.ymgmr.2019.100512.
26. Dutto, I.; Gerhards, J.; Herrera, A.; Souckova, O.; Škopová, V.; Smak, J.A.; Junza, A.; Yanes, O.; Boeckx, C.; Burkhalter, M.D.; et al. Pathway-Specific Effects of ADSL Deficiency on Neurodevelopment. *eLife* **2022**, *11*, e70518, doi:10.7554/eLife.70518.
27. Marsac, R.; Pinson, B.; Saint-Marc, C.; Olmedo, M.; Artal-Sanz, M.; Daignan-Fornier, B.; Gomes, J.-E. Purine Homeostasis Is Necessary for Developmental Timing, Germline Maintenance and Muscle Integrity in Caenorhabditis Elegans. *Genetics* **2019**, *211*, 1297–1313, doi:10.1534/genetics.118.301062.
28. Sater, A.K.; Moody, S.A. Using Xenopus to Understand Human Disease and Developmental Disorders. *Genes. N. Y. N 2000* **2017**, *55*, doi:10.1002/dvg.22997.
29. Blum, M.; Ott, T. Xenopus: An Undervalued Model Organism to Study and Model Human Genetic Disease. *Cells Tissues Organs* **2018**, *205*, 303–313, doi:10.1159/000490898.
30. Garí, E.; Piedrafita, L.; Aldea, M.; Herrero, E. A Set of Vectors with a Tetracycline-Regulatable Promoter System for Modulated Gene Expression in Saccharomyces Cerevisiae. *Yeast Chichester Engl.* **1997**, *13*, 837–848, doi:10.1002/(SICI)1097-0061(199707)13:9<837::AID-YEA145>3.0.CO;2-T.

31. Nieuwkoop, P.D.; Faber, J. *Normal Table of Xenopus Laevis (Daudin): A Systematical and Chronological Survey of the Development from the Fertilized Egg Till the End of Metamorphosis*; Garland Pub., 1994; ISBN 978-0-8153-1896-5.
32. Massé, K.; Bhamra, S.; Eason, R.; Dale, N.; Jones, E.A. Purine-Mediated Signalling Triggers Eye Development. *Nature* **2007**, *449*, 1058–1062, doi:10.1038/nature06189.
33. Blanchard, C.; Boué-Grabot, E.; Massé, K. Comparative Embryonic Spatio-Temporal Expression Profile Map of the Xenopus P2X Receptor Family. *Front. Cell. Neurosci.* **2019**, *13*, 340, doi:10.3389/fncel.2019.00340.
34. Massé, K.; Eason, R.; Bhamra, S.; Dale, N.; Jones, E.A. Comparative Genomic and Expression Analysis of the Conserved NTPDase Gene Family in Xenopus. *Genomics* **2006**, *87*, 366–381, doi:10.1016/j.ygeno.2005.11.003.
35. Della Gaspera, B.; Armand, A.-S.; Lecolle, S.; Charbonnier, F.; Chanoine, C. Mef2d Acts Upstream of Muscle Identity Genes and Couples Lateral Myogenesis to Dermomyotome Formation in Xenopus Laevis. *PloS One* **2012**, *7*, e52359, doi:10.1371/journal.pone.0052359.
36. Della Gaspera, B.; Armand, A.-S.; Sequeira, I.; Chesneau, A.; Mazabraud, A.; Lécolle, S.; Charbonnier, F.; Chanoine, C. Myogenic Waves and Myogenic Programs during Xenopus Embryonic Myogenesis. *Dev. Dyn. Off. Publ. Am. Assoc. Anat.* **2012**, *241*, 995–1007, doi:10.1002/dvdy.23780.
37. Martin, B.L.; Harland, R.M. A Novel Role for Lbx1 in Xenopus Hypaxial Myogenesis. *Dev. Camb. Engl.* **2006**, *133*, 195–208, doi:10.1242/dev.02183.
38. Kintner, C.R.; Brockes, J.P. Monoclonal Antibodies Identify Blastemal Cells Derived from Dedifferentiating Limb Regeneration. *Nature* **1984**, *308*, 67–69, doi:10.1038/308067a0.
39. Massé, K.; Bhamra, S.; Allsop, G.; Dale, N.; Jones, E.A. Ectophosphodiesterase/Nucleotide Phosphohydrolase (Enpp) Nucleotidases: Cloning, Conservation and Developmental Restriction. *Int. J. Dev. Biol.* **2010**, *54*, 181–193, doi:10.1387/ijdb.092879km.
40. Bassez, T.; Paris, J.; Omilli, F.; Dorel, C.; Osborne, H.B. Post-Transcriptional Regulation of Ornithine Decarboxylase in Xenopus Laevis Oocytes. *Dev. Camb. Engl.* **1990**, *110*, 955–962.
41. Bowes, J.B.; Snyder, K.A.; Segerdell, E.; Gibb, R.; Jarabek, C.; Noumen, E.; Pollet, N.; Vize, P.D. Xenbase: A Xenopus Biology and Genomics Resource. *Nucleic Acids Res.* **2008**, *36*, D761-767, doi:10.1093/nar/gkm826.
42. Karpinka, J.B.; Fortriede, J.D.; Burns, K.A.; James-Zorn, C.; Ponferrada, V.G.; Lee, J.; Karimi, K.; Zorn, A.M.; Vize, P.D. Xenbase, the Xenopus Model Organism Database; New Virtualized System, Data Types and Genomes. *Nucleic Acids Res.* **2015**, *43*, D756-763, doi:10.1093/nar/gku956.
43. Session, A.M.; Uno, Y.; Kwon, T.; Chapman, J.A.; Toyoda, A.; Takahashi, S.; Fukui, A.; Hikosaka, A.; Suzuki, A.; Kondo, M.; et al. Genome Evolution in the Allotetraploid Frog Xenopus Laevis. *Nature* **2016**, *538*, 336–343, doi:10.1038/nature19840.
44. Ljungdahl, P.O.; Daignan-Fornier, B. Regulation of Amino Acid, Nucleotide, and Phosphate Metabolism in Saccharomyces Cerevisiae. *Genetics* **2012**, *190*, 885–929, doi:10.1534/genetics.111.133306.
45. Kragtorp, K.A.; Miller, J.R. Integrin Alpha5 Is Required for Somite Rotation and Boundary Formation in Xenopus. *Dev. Dyn. Off. Publ. Am. Assoc. Anat.* **2007**, *236*, 2713–2720, doi:10.1002/dvdy.21280.
46. Moreno, T.A.; Kintner, C. Regulation of Segmental Patterning by Retinoic Acid Signaling during Xenopus Somitogenesis. *Dev. Cell* **2004**, *6*, 205–218, doi:10.1016/s1534-5807(04)00026-7.

47. Sparrow, D.B.; Jen, W.C.; Kotecha, S.; Towers, N.; Kintner, C.; Mohun, T.J. Thylacine 1 Is Expressed Segmentally within the Paraxial Mesoderm of the Xenopus Embryo and Interacts with the Notch Pathway. *Dev. Camb. Engl.* **1998**, *125*, 2041–2051, doi:10.1242/dev.125.11.2041.
48. Tocco, A.; Pinson, B.; Thiébaud, P.; Thézé, N.; Massé, K. Comparative Genomic and Expression Analysis of the Adenosine Signaling Pathway Members in Xenopus. *Purinergic Signal.* **2015**, *11*, 59–77, doi:10.1007/s11302-014-9431-6.
49. Della Gaspera, B.; Weill, L.; Chanoine, C. Evolution of Somite Compartmentalization: A View From Xenopus. *Front. Cell Dev. Biol.* **2021**, *9*, 790847, doi:10.3389/fcell.2021.790847.
50. Wilson-Rawls, J.; Hurt, C.R.; Parsons, S.M.; Rawls, A. Differential Regulation of Epaxial and Hypaxial Muscle Development by Paraxis. *Dev. Camb. Engl.* **1999**, *126*, 5217–5229, doi:10.1242/dev.126.23.5217.
51. Martin, B.L.; Harland, R.M. Hypaxial Muscle Migration during Primary Myogenesis in Xenopus Laevis. *Dev. Biol.* **2001**, *239*, 270–280, doi:10.1006/dbio.2001.0434.
52. Kelley, R.E.; Andersson, H.C. Disorders of Purines and Pyrimidines. *Handb. Clin. Neurol.* **2014**, *120*, 827–838, doi:10.1016/B978-0-7020-4087-0.00055-3.
53. Iijima, R.; Kunieda, T.; Yamaguchi, S.; Kamigaki, H.; Fujii-Taira, I.; Sekimizu, K.; Kubo, T.; Natori, S.; Homma, K.J. The Extracellular Adenosine Deaminase Growth Factor, ADGF/CECR1, Plays a Role in Xenopus Embryogenesis via the Adenosine/P1 Receptor. *J. Biol. Chem.* **2008**, *283*, 2255–2264, doi:10.1074/jbc.M709279200.
54. Maguire, R.J.; Isaacs, H.V.; Pownall, M.E. Early Transcriptional Targets of MyoD Link Myogenesis and Somitogenesis. *Dev. Biol.* **2012**, *371*, 256–268, doi:10.1016/j.ydbio.2012.08.027.
55. Kim, P.B.; Nelson, J.W.; Breaker, R.R. An Ancient Riboswitch Class in Bacteria Regulates Purine Biosynthesis and One-Carbon Metabolism. *Mol. Cell* **2015**, *57*, 317–328, doi:10.1016/j.molcel.2015.01.001.
56. Nakagawara, K.; Takeuchi, C.; Ishige, K. 5’-CMP and 5’-UMP Promote Myogenic Differentiation and Mitochondrial Biogenesis by Activating Myogenin and PGC-1α in a Mouse Myoblast C2C12 Cell Line. *Biochem. Biophys. Rep.* **2022**, *31*, 101309, doi:10.1016/j.bbrep.2022.101309.
57. Sabillo, A.; Ramirez, J.; Domingo, C.R. Making Muscle: Morphogenetic Movements and Molecular Mechanisms of Myogenesis in Xenopus Laevis. *Semin. Cell Dev. Biol.* **2016**, *51*, 80–91, doi:10.1016/j.semcdb.2016.02.006.
58. Knight, J.D.; Kothary, R. The Myogenic Kinome: Protein Kinases Critical to Mammalian Skeletal Myogenesis. *Skelet. Muscle* **2011**, *1*, 29, doi:10.1186/2044-5040-1-29.
59. Burnstock, G.; Arnett, T.R.; Orriss, I.R. Purinergic Signalling in the Musculoskeletal System. *Purinergic Signal.* **2013**, *9*, 541–572, doi:10.1007/s11302-013-9381-4.
60. Pietrangelo, T.; Guarnieri, S.; Fulle, S.; Fanò, G.; Mariggiò, M.A. Signal Transduction Events Induced by Extracellular Guanosine 5’ Triphosphate in Excitable Cells. *Purinergic Signal.* **2006**, *2*, 633–636, doi:10.1007/s11302-006-9021-3.
61. Meyer, M.P.; Gröschel-Stewart, U.; Robson, T.; Burnstock, G. Expression of Two ATP-Gated Ion Channels, P2X5 and P2X6, in Developing Chick Skeletal Muscle. *Dev. Dyn. Off. Publ. Am. Assoc. Anat.* **1999**, *216*, 442–449, doi:10.1002/(SICI)1097-0177(199912)216:4/5<442::AID-DVDY12>3.0.CO;2-Z.
62. Ryten, M.; Dunn, P.M.; Neary, J.T.; Burnstock, G. ATP Regulates the Differentiation of Mammalian Skeletal Muscle by Activation of a P2X5 Receptor on Satellite Cells. *J. Cell Biol.* **2002**, *158*, 345–355, doi:10.1083/jcb.200202025.

63. Maire, P.; Dos Santos, M.; Madani, R.; Sakakibara, I.; Viaut, C.; Wurmser, M. Myogenesis Control by SIX Transcriptional Complexes. *Semin. Cell Dev. Biol.* **2020**, *104*, 51–64, doi:10.1016/j.semcdb.2020.03.003.
64. Janesick, A.; Tang, W.; Nguyen, T.T.L.; Blumberg, B. RARβ2 Is Required for Vertebrate Somitogenesis. *Dev. Camb. Engl.* **2017**, *144*, 1997–2008, doi:10.1242/dev.144345.
65. Chen, J.; Li, Q. Implication of Retinoic Acid Receptor Selective Signaling in Myogenic Differentiation. *Sci. Rep.* **2016**, *6*, 18856, doi:10.1038/srep18856.
66. Baló-Banga, J.M.; Leibinger, J.; Molnár, L.; Király, K. The Effect of Retinoic Acid on the Synthesis of Phosphoribosylpyrophosphate in Human Erythrocytes in Psoriasis. A Preliminary Note. *Dermatologica* **1978**, *157 Suppl 1*, 45–51, doi:10.1159/000250884.
67. Paschaki, M.; Schneider, C.; Rhinn, M.; Thibault-Carpentier, C.; Dembélé, D.; Niederreither, K.; Dollé, P. Transcriptomic Analysis of Murine Embryos Lacking Endogenous Retinoic Acid Signaling. *PloS One* **2013**, *8*, e62274, doi:10.1371/journal.pone.0062274.

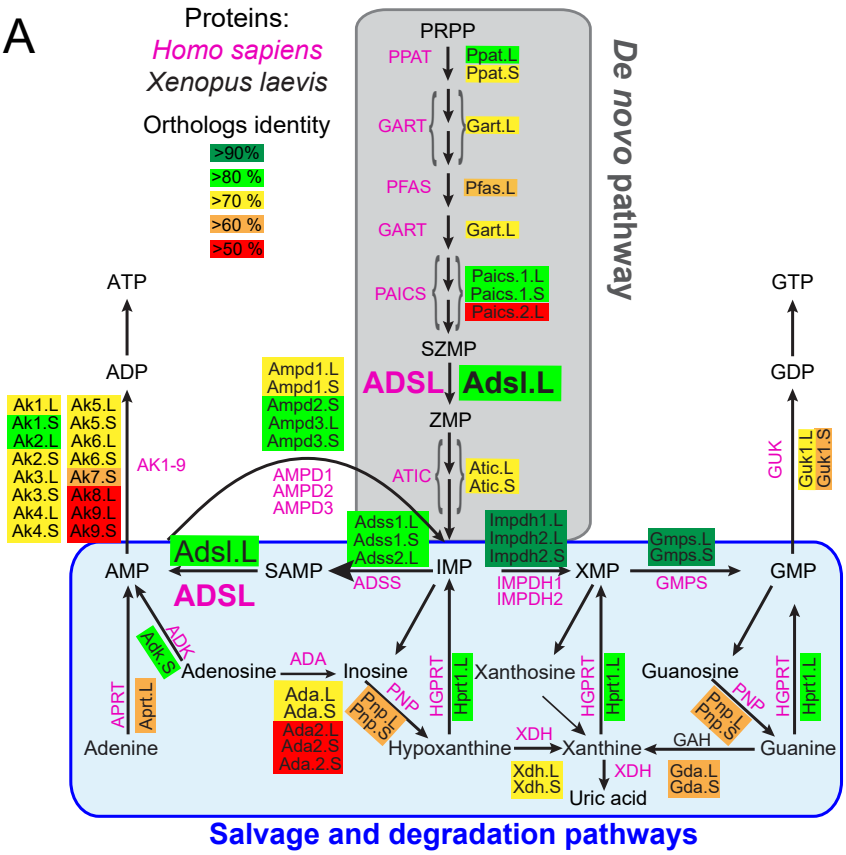

Figure 1. The *X. laevis adsl.L* gene encodes the adenylosuccinate lyase activity required in two non-sequential steps of the highly conserved purine synthesis pathways. (**A**) Schematic representation of the human and *X. laevis* purine biosynthesis pathways. Abbreviations: AMP: adenosine monophosphate; GMP: guanosine monophosphate; IMP: Inosine monophosphate; PRPP: Phosphorybosyl pyrophosphate; SAMP: Succinyl-AMP; SZMP: Succinyl-Amino Imidazole Carboxamide Ribonucleotide monophosphate; XMP: Xanthosine monophosphate; ZMP: Amino Imidazole CarboxAmide Ribonucleotide monophosphate. (**B**) Functional complementation of the growth defect of the yeast adenylosuccinate lyase deletion mutant by expression of the *X. laevis adsl.L* ortholog gene. Yeast wild-type and *adsl* knock-out mutant (*ade13 ade1*) strains were either transformed with a plasmid allowing expression of the *Saccharomyces cerevisiae* (*ADE13*) or the *X. laevis* (*adsl.L*) adenylosuccinate lyase encoding genes, or with the empty vector (None). Serial dilutions (1/10) of transformants were dropped on SDcasaWA medium supplemented with either hypoxanthine or adenine as the sole external purine source. Plates were incubated for 48 h at 37 °C before imaging. Of note the *ade1 ade13* double deletion mutant was used in this experiment to avoid genetic instability associated with the accumulation of SZMP and/or its nucleoside derivatives observed in the single *ade13* single mutant [8].

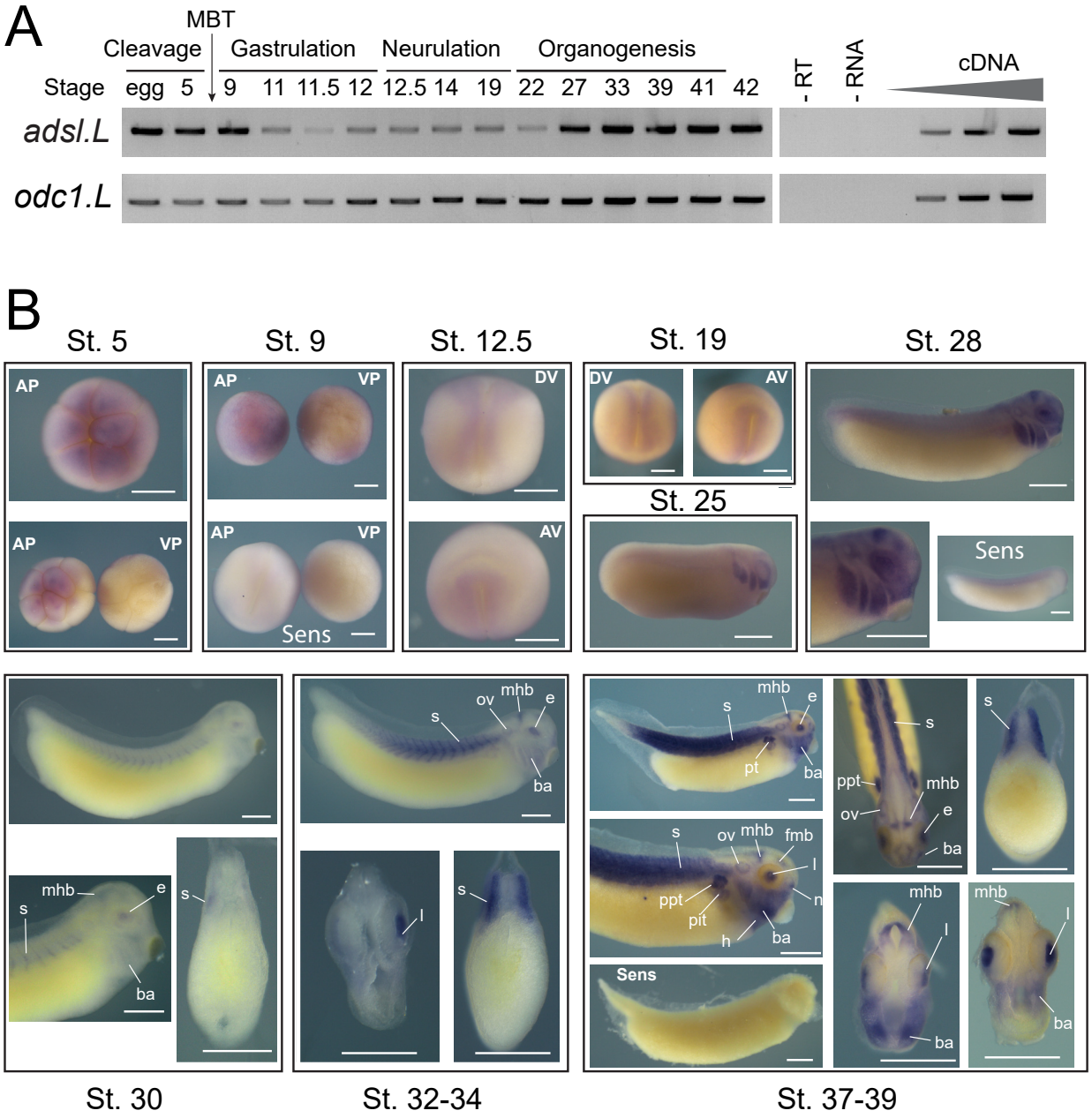

Figure 2. Spatiotemporal expression of *adsl.L* gene during *X. laevis* embryonic development. (**A**) Temporal expression profiles of *adsl.L* gene during embryogenesis. The expression profile was determined by RT-PCR from the cDNA of the fertilized oocyte (egg) and whole embryo at indicated stages covering the different phases of *X. laevis* embryogenesis. The ornithine decarboxylase gene *odc1.L* was used as a loading control and negative controls were performed by omitting either reverse transcriptase (-RT) or RNA (-RNA) in the reaction mix. Linearity was determined by dilutions of cDNA from stage 39 for *adsl.L* and 41 for *odc1.L*. Mid-blastula transition (MBT) is indicated. (**B**) Spatial expression profile of *adsl.L* gene during embryogenesis. Whole-mount *in situ* hybridization with *adsl.L*-specific DIG-labelled antisense or sense RNA probes was performed on embryos from stages (St.) 5 to 37/39. St. 5 and 9: animal (AP) and vegetal (VP) pole views, St. 12.5 and 19: dorsal (DV) and anterior (AV) views; later stages: lateral views, with dorsal up and anterior on the right, and dorsal view at stage 37-39. Transverse sections are dorsal up. Abbreviations: ba, branchial arches; e, eye; fmb, forebrain-midbrain boundary; h, heart; l, lens; mhb, midbrain-hindbrain boundary; n: nasal placode; ov, otic vesicle; ppt, pronephric proximal tubules; pit, pronephric intermediate tubules; s, somites. Bars: 0.5 mm.

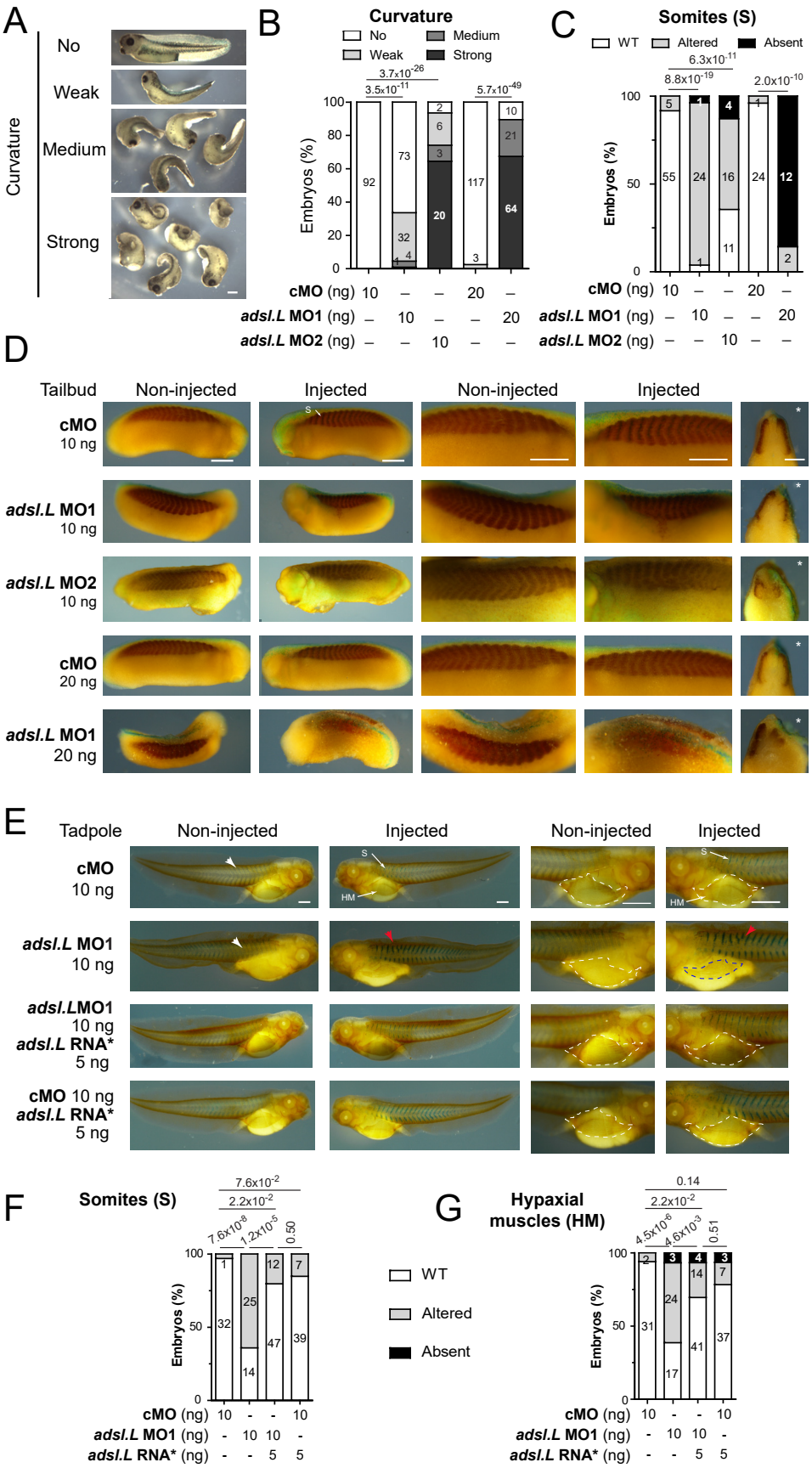

Figure 3. The *adsl.L* gene is required for somites and hypaxial muscle formation in *X. laevis*. (**A**) Representative images of *adsl.L* morphants following *adsl.L* MO1 injection at either 10 ng (weak and medium curvature) or 20 ng (medium and strong curvature). (**B**) Quantification and statistics of the curvature phenotype. (**C-G**) Immunostaining with the differentiated muscle cells specific 12-101 antibody revealed a strong alteration of somites and hypaxial muscle formation in *adsl.L* knock-down and *adsl.L* over-expressing embryos. Representative images (**D-E**), quantification and statistics (**C**, **F-G**) of somites and hypaxial muscles phenotype at tailbud (**C-D**) and tadpole (**E-G**) stages. Injected side is indicated by asterisks. S: somites; HM: Hypaxial muscles. Bars: 0.5 mm. White and red arrowheads point to typical somite chevron shapes and altered somites, respectively. The a*dsl.L* RNA* refers to mutated RNA whose translation is not affected by the *adsl.L* specific MOs (Figure S3). Numbers above the bars of histograms correspond to p-values.

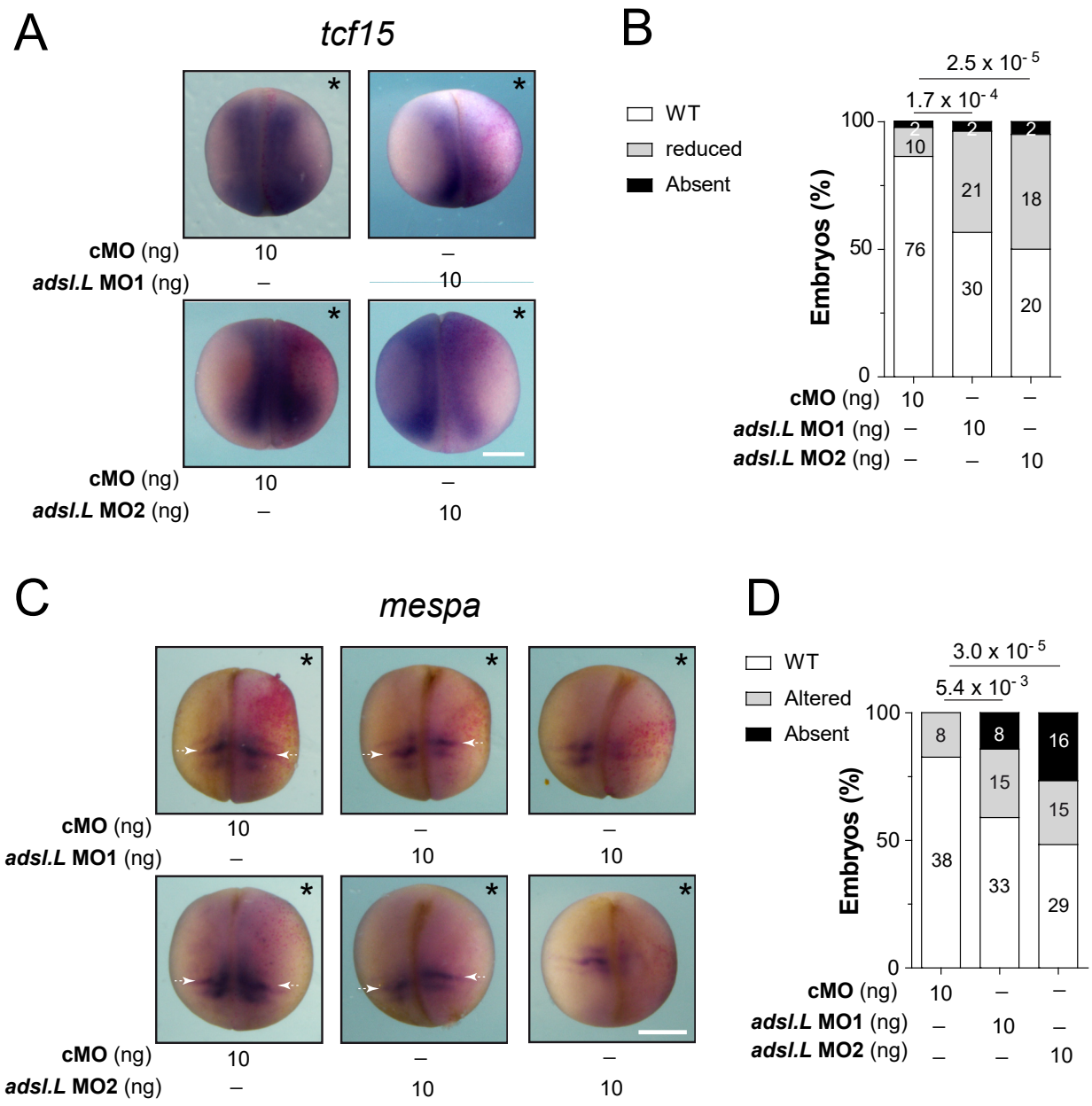

Figure 4. The *adsl.L* gene is required for the expression of *tcf15* and *mespa* genes involved in in early somitogenesis. Expression of *tcf15* (**A-B**) and *mespa* (**C-D**) genes at late neurula stage is altered by the knock-down of *adsl.L* gene. Representative images of *trf15* (**A**) and *mespa* (**C**) RNA expression revealed by *in situ* hybridization. Statistics are shown in **B** and **D** for *trf15* and *mespa* RNA, respectively. White arrows point to the anterior domain of the somitomere S-II on both side of the embryos. Injected side is indicated by asterisks. Numbers above the bars of histograms correspond to p-values. Bars: 0.5 mm.

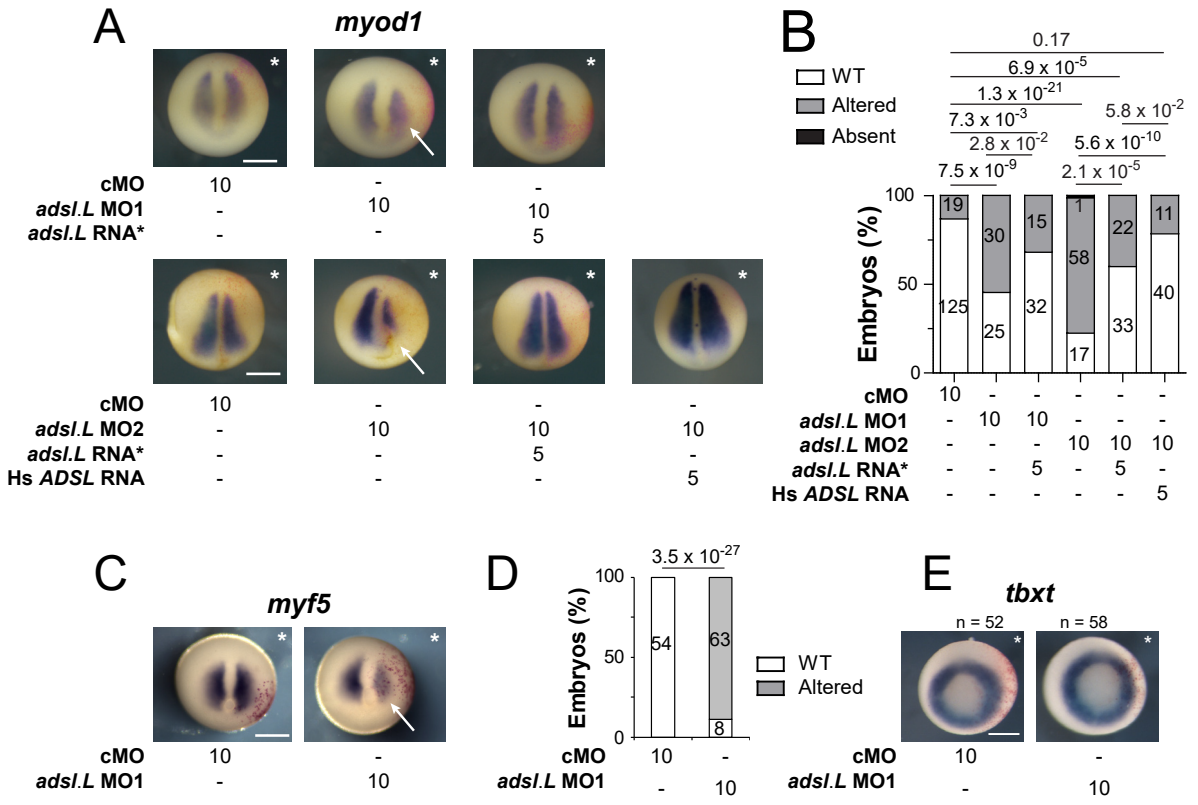

Figure 5. Expression of the myogenic regulatory factors *myod1* and *myf5* in paraxial mesoderm is strongly affected by the knock-down of the *adsl.L* gene. (**A**) Expression of *myod1* gene at the early neurula stage is altered by the knock-down of *adsl.L* gene and rescued by *adsl.L* RNA* and human *ADSL* RNA. (**C**) Representative images of the effect on *myf5* RNA expression by *adsl.L* knock-down at stage 12.5 revealed by *in situ* hybridization. (**B, D**) Quantification and statistics of the *myod1* and *myf5* expression phenotypes are presented in (**A**) and (**C**), respectively. (**E**) Knock-down of *adsl.L* does not alter mesoderm formation, as revealed by the absence of change in *tbxt* (*xbra*) RNA expression domain at stage 11. Injected side is indicated by asterisks. The amounts of MO and RNA presented in this figure are in ng. Bars: 0.5 mm. Numbers above the bars of histograms correspond to p-values.

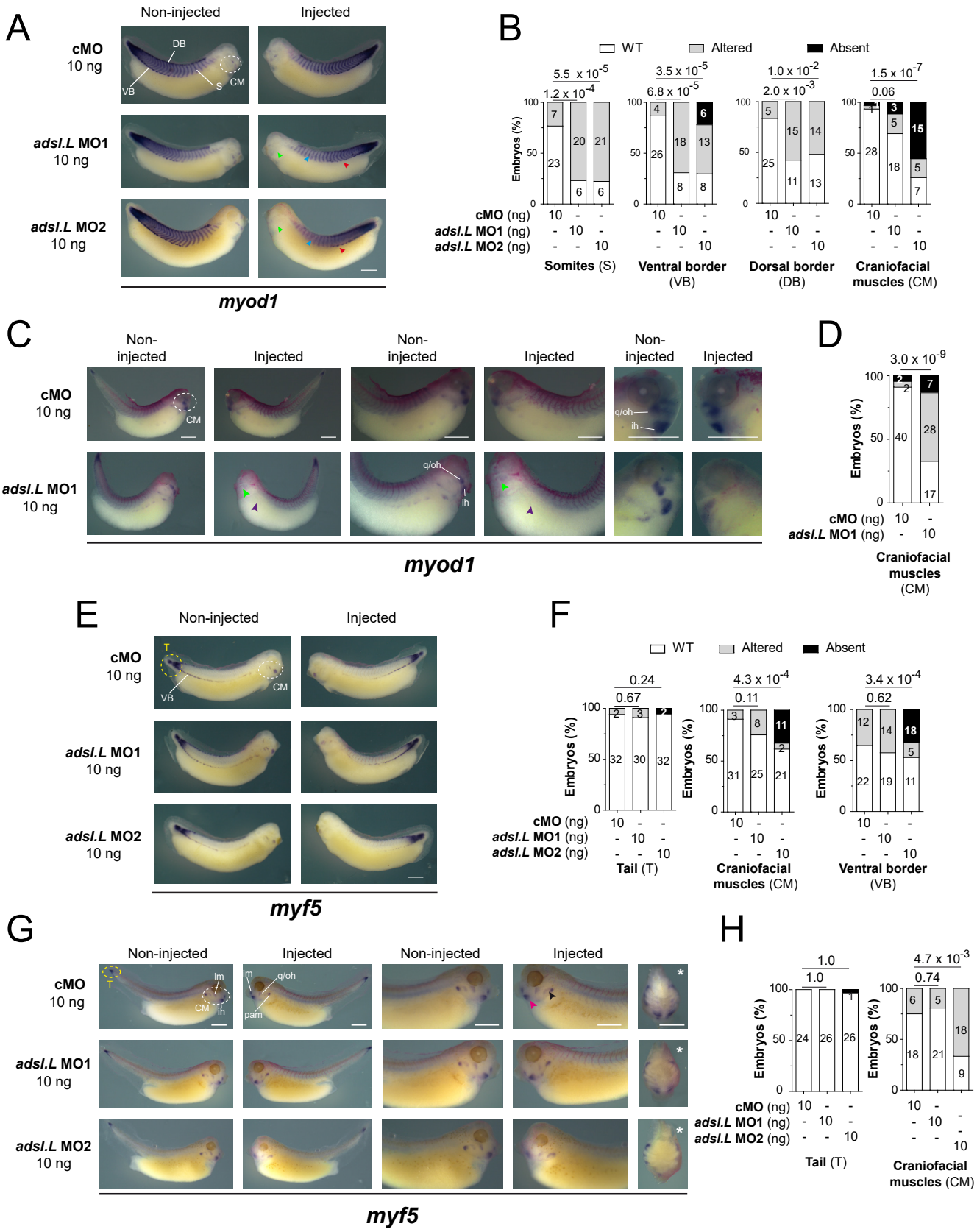

Figure 6. Knock-down of *adsl.L* gene causes an impaired expression of *myod1* and *myf5* at late tailbud and tadpole embryonic stages leading to somites and craniofacial muscle formation defects. (A-D) Representative images of the *adsl.L*-dependent altered expression of *myod1* (A) and *myf5* (C) domains in either somite (S), dorsal somite border (DB), ventral somite border (VB) or craniofacial muscles (CM), as revealed by *in situ* hybridization in late tailbud embryos. (E, G) Representative images of the *adsl.L*-dependent altered expression of *myod1* (E) and *myf5* (G) domains in the unsegmented mesoderm in the most posterior tail (T), somites (S), ventral somite border (VB) and craniofacial muscles (CM) in tadpole embryos. (B, D, F, H) Quantification and statistics of the *myod1* and *myf5* expression phenotypes are presented in (A), (C), (E) and (G), respectively. Craniofacial muscles: ih, interhyoïedus anlage; im, intermandibularis anlage; lm, levatores mandibulae anlage; pam, pharyngeal archmuscle anlagen; q/oh, common orbitohyoïdeus and quadrato-hyoangularis precursors. Injected side is indicated by asterisks. Bars: 0.5 mm. Numbers above the bars of histograms correspond to p-values.

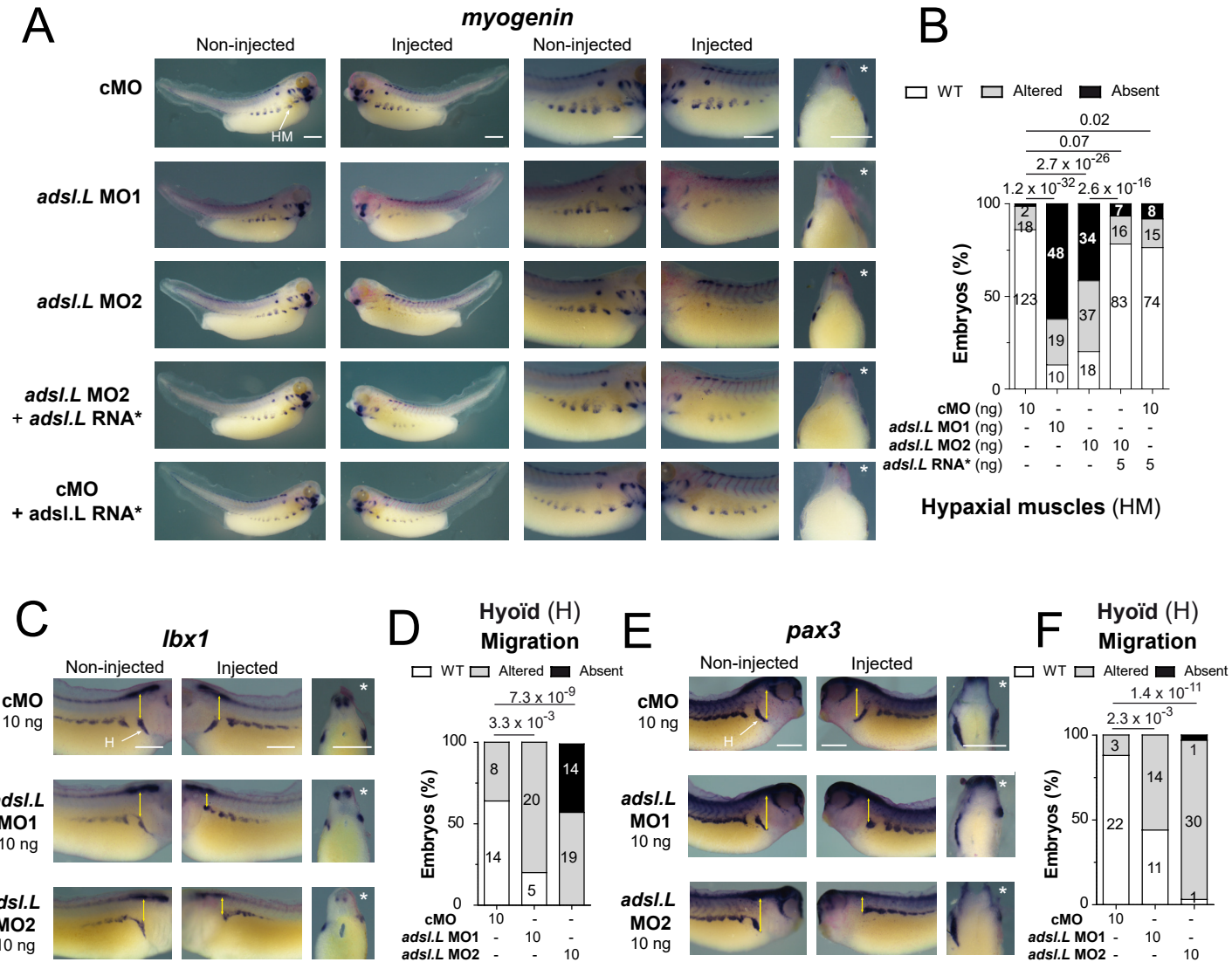

Figure 7. The *adsl.L* gene is required for hypaxial muscle migration. (**A-B**) The hypaxial muscle defect associated with *adsl.L* knock-down is rescued by the MO non-targeted *adsl.L* RNA*. Representative images (**A**), quantifications (number in bars) and statistics (**B**) of the *adsl.L*-dependent alteration of *myogenin* gene expression monitored by *in situ* hybridization. (**C-F**) Migration of myoblasts in the hyoid region is found severely affected in *adsl.L* morphants as shown by *lbx1* (**C-D**) and *pax3* genes expression pattern alteration (**E-F**). Injected side is indicated by asterisks. Bars: 0.5 mm. HM and H stand for hypaxial muscles and hyoid region, respectively Numbers above the bars of histograms correspond to p-values.

Supplementary Materials

Purine biosynthesis pathways are required for embryonic myogenesis in *Xenopus laevis*

Maëlle Duperray, Fanny Hardet, Elodie Henriet, Christelle Saint-Marc, Eric Boué-Grabot, Bertrand Daignan-Fornier, Karine Massé and Benoît Pinson

Supplementary Figures

Supplementary Tables

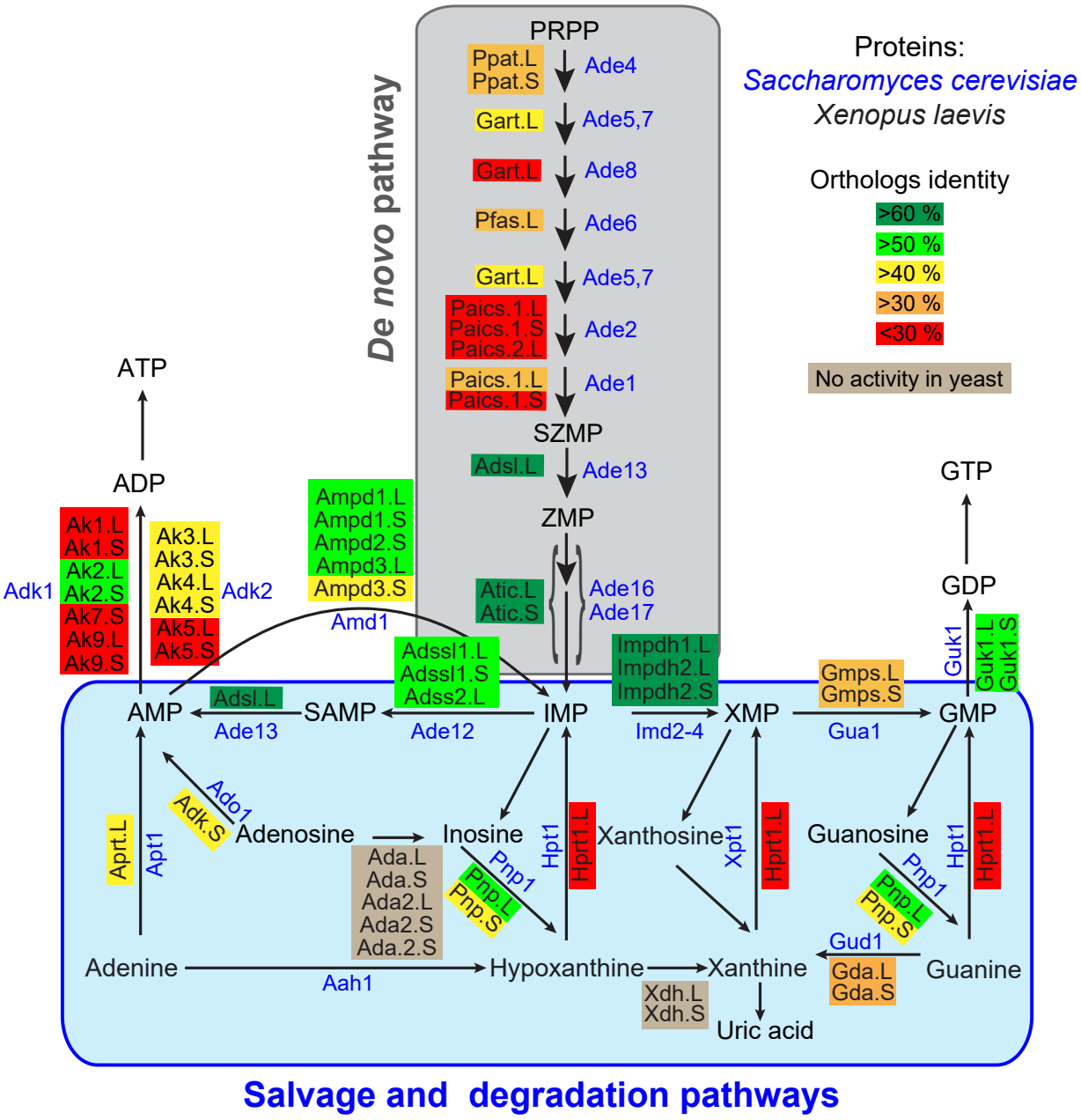

Figure S1. Conservation of purine biosynthesis pathways between the yeast *Saccharomyces cerevisiae* and *Xenopus laevis*. Features of the *X. laevis* and yeast enzymes are listed in Table S7. Abbreviations: AMP: adenosine monophosphate; GMP: guanosine monophosphate; IMP: Inosine monophosphate; PRPP: Phosphoribosyl pyrophosphate; SAMP: Succinyl-AMP; SZMP: Succinyl Amino Imidazole Carboxamide Ribonucleotide monophosphate; XMP: Xanthosine monophosphate; ZMP: Amino Imidazole CarboxAmide Ribonucleotide monophosphate.

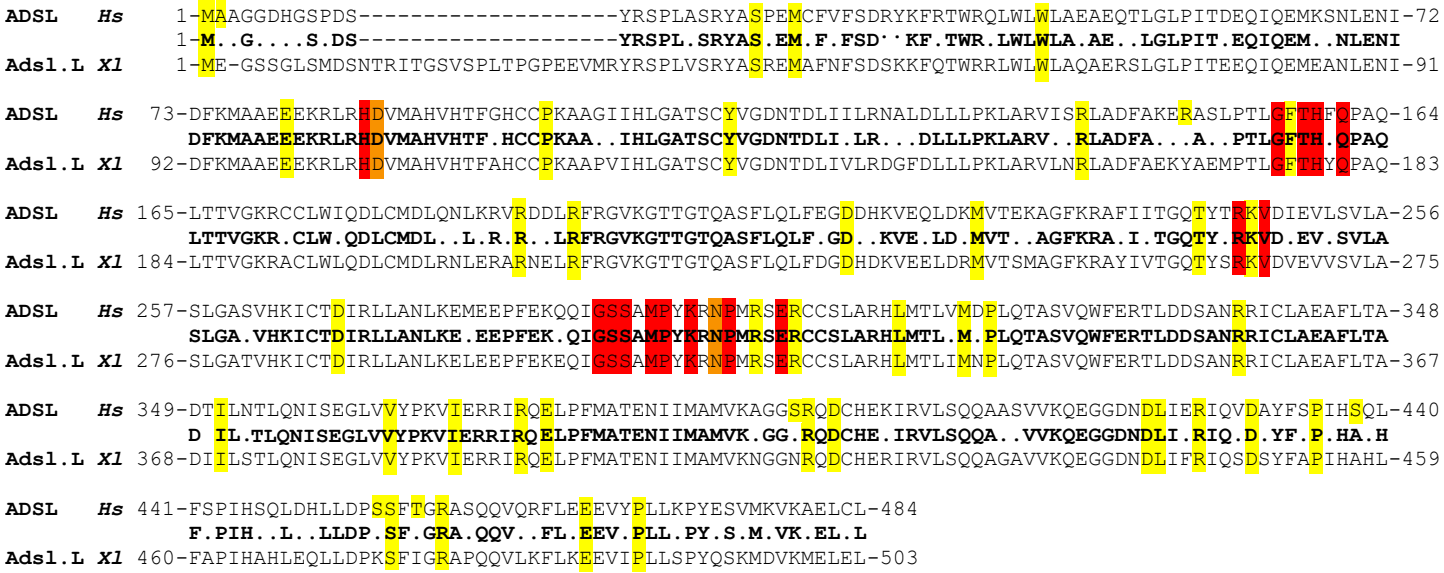

Figure S2. Sequence comparison between the *H. sapiens* (*Hs*) and *X. laevis* (*Xl*) adenylosuccinate lyase enzymes. Conserved amino acids are indicated in bold. Red and orange boxes point to residues required for catalysis and yellow and orange boxes to mutated residues found in *ADSL*-deficient patients.

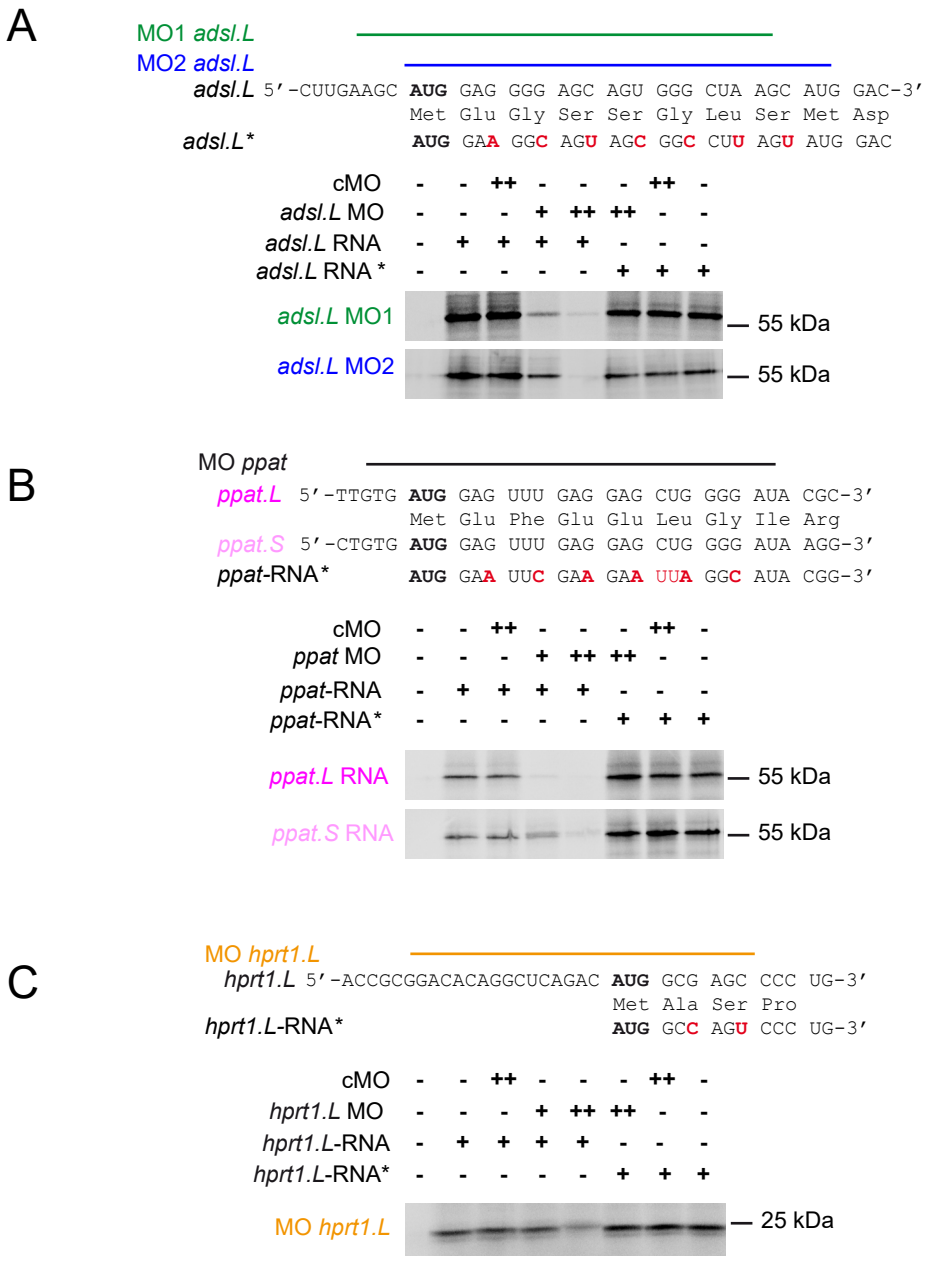

Figure S3. Validation of the morpholinos translation interference by *in vitro* translation. The *adsl.L* (**A**), *ppat.L/ppat.S* (**B**) and *hprt1.L* (**C**) RNAs were produced using the *mMessage mMachine SP6* kit (ambion) according to the supplier procedure. *In vitro* translation was then performed by using the reticulocyte rabbit lysate system kit (Promega) in 25 µl reaction mix containing 500 ng of indicated RNA, 0.5 µl of the amino acid mix w/o Met (1 mM), 2 µl of [^{35}S]-methionine (1,200 Ci/mmol; 10 mCi/ml), 17.5 µl of the reticulocytes lysate, 0.5 µL of RNAse inhibitor (40 u/µl; Promega) and in the presence or the absence of 40 (+) or 400 (++) ng of indicated Morpholino (MO). Proteins were separated by SDS-PAGE and radiolabeled proteins were detected by phosphorimaging (Typhoon biomolecular imager, Amersham). RNA* refers to mutated RNAs whose translation is not affected by the gene-specific MOs.

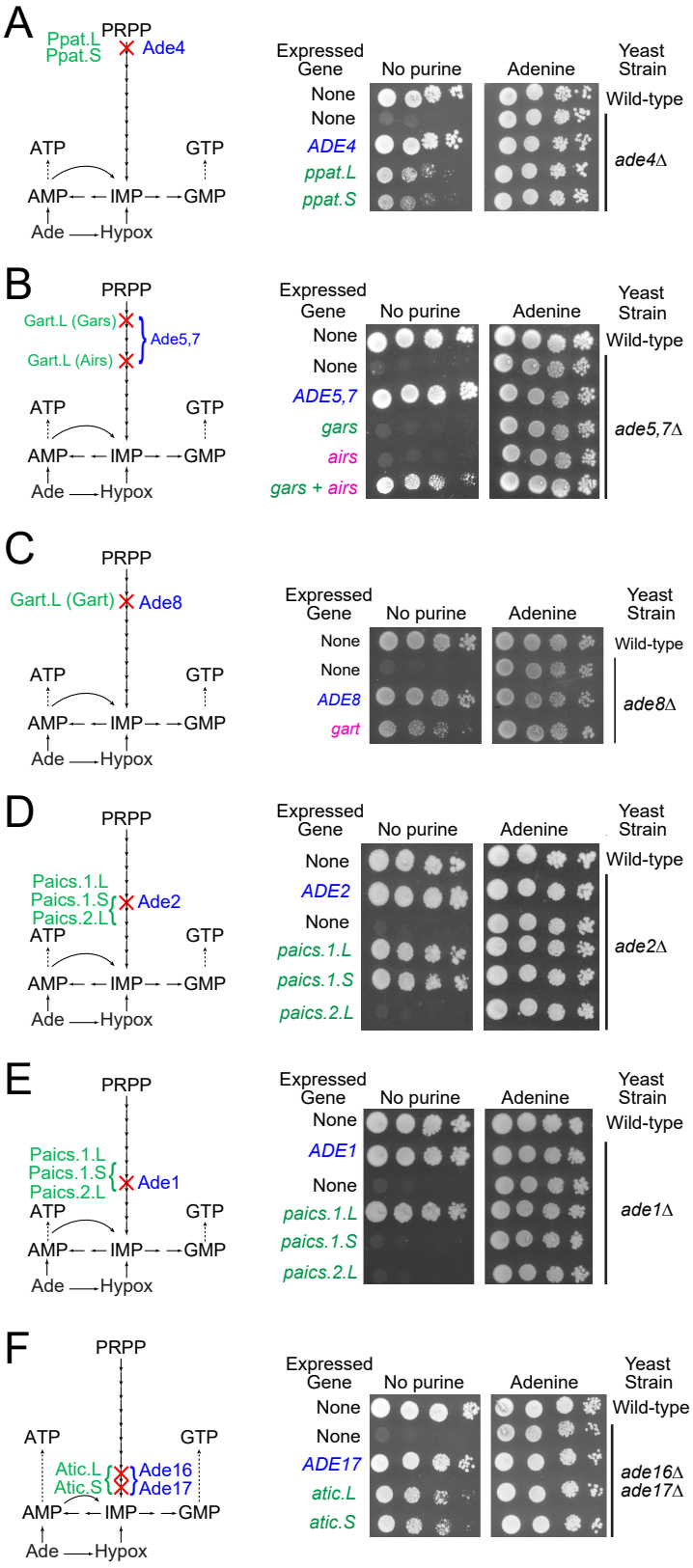

Figure S4. Functional complementation of yeast purine *de novo* pathway mutants by the *X. laevis* ortholog genes. Red crosses indicate the purine pathway steps knocked-out in each yeast mutant. *S. cerevisiae*, *X. laevis* and *X. tropicalis* protein or gene names are written in blue, green and pink, respectively. For Airs and Gart activities, functional complementation was performed by expressing the *X. tropicalis* corresponding open reading frames. Abbreviations: Ade: adenine; Airs; aminoimidazole ribonucleotide synthetase activity; Gars: glycinamide ribonucleotide synthetase activity; Gart: glycinamide ribonucleotide transformylase activity; Hypox: hypoxanthine; IMP: Inosine monophosphate; PRPP: Phosphorybosyl pyrophosphate. Yeast mutants were transformed with plasmids allowing expression of the indicated yeast (blue) or *X. laevis* (green) or *X. tropicalis* (pink) genes or with the empty vector (None). Transformants were serial (1/10) diluted and spotted on SDcasaW medium supplemented or not (no purine) with adenine as sole external purine source. Plates were imaged after 2 (**F**), 4 (**A**, **D-E**) or 7 days (**B-C**) at either 30°C (**A**, **D-F**) or 37°C (**B-C**).

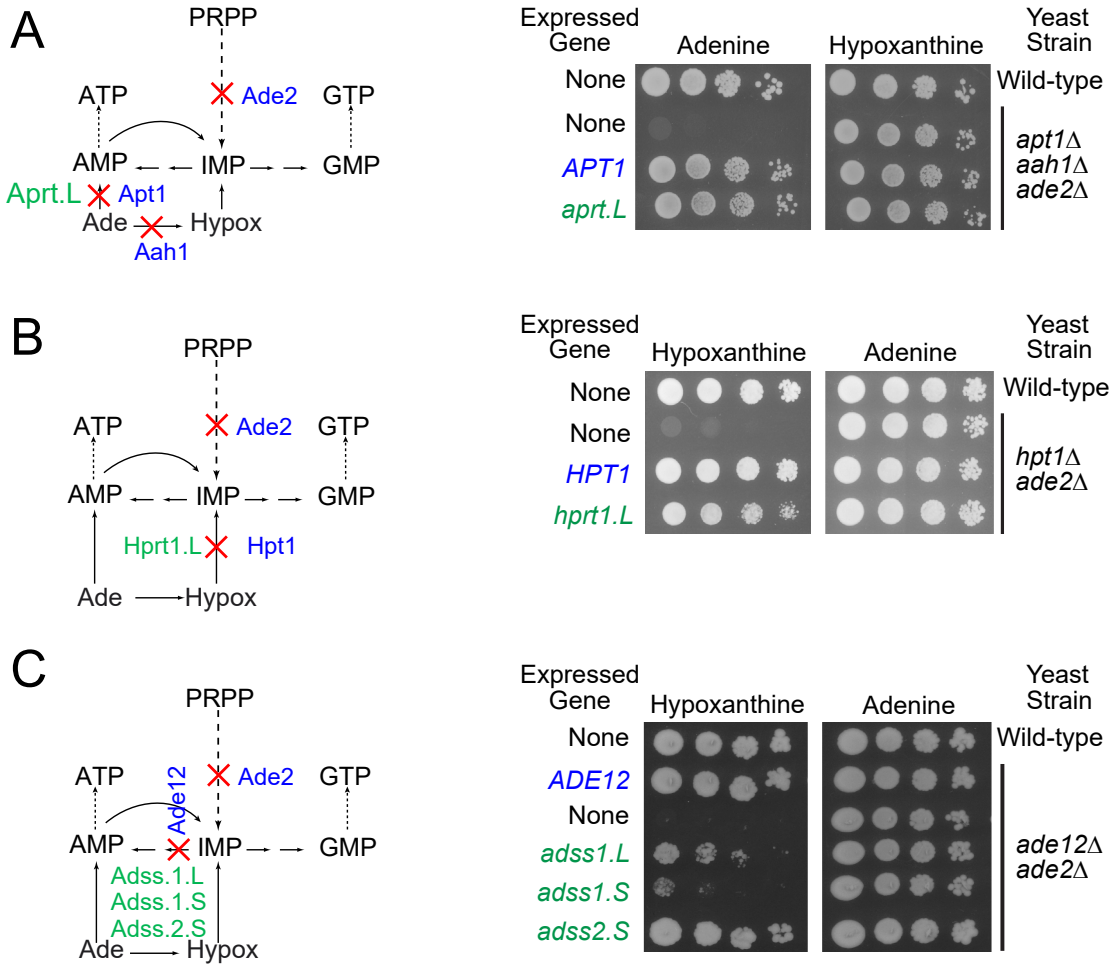

Figure S5. Functional complementation of yeast purine salvage knocked-out mutants by the *X. laevis* ortholog genes. The vertical dashed line symbolizes the *de novo* purine pathway. Red crosses are used to indicate the purine pathway steps absent in each yeast knock-out mutant. *S. cerevisiae* and *X. laevis* protein or gene names are written in blue and green, respectively. Ade: Adenine; Hypox: Hypoxanthine; IMP: Inosine monophosphate; PRPP: 5-phosphorybosyl-pyrophosphate. Wild-type and mutant yeast strains were transformed with plasmids allowing expression of the indicated *S. cerevisiae* (blue) or *X. laevis* (green) genes or with the empty vector (None). Transformants were serial diluted (1/10) and spotted on SDcasaW medium supplemented with either adenine or hypoxanthine as sole external purine source. Plates were imaged after 2 days at 30°C.

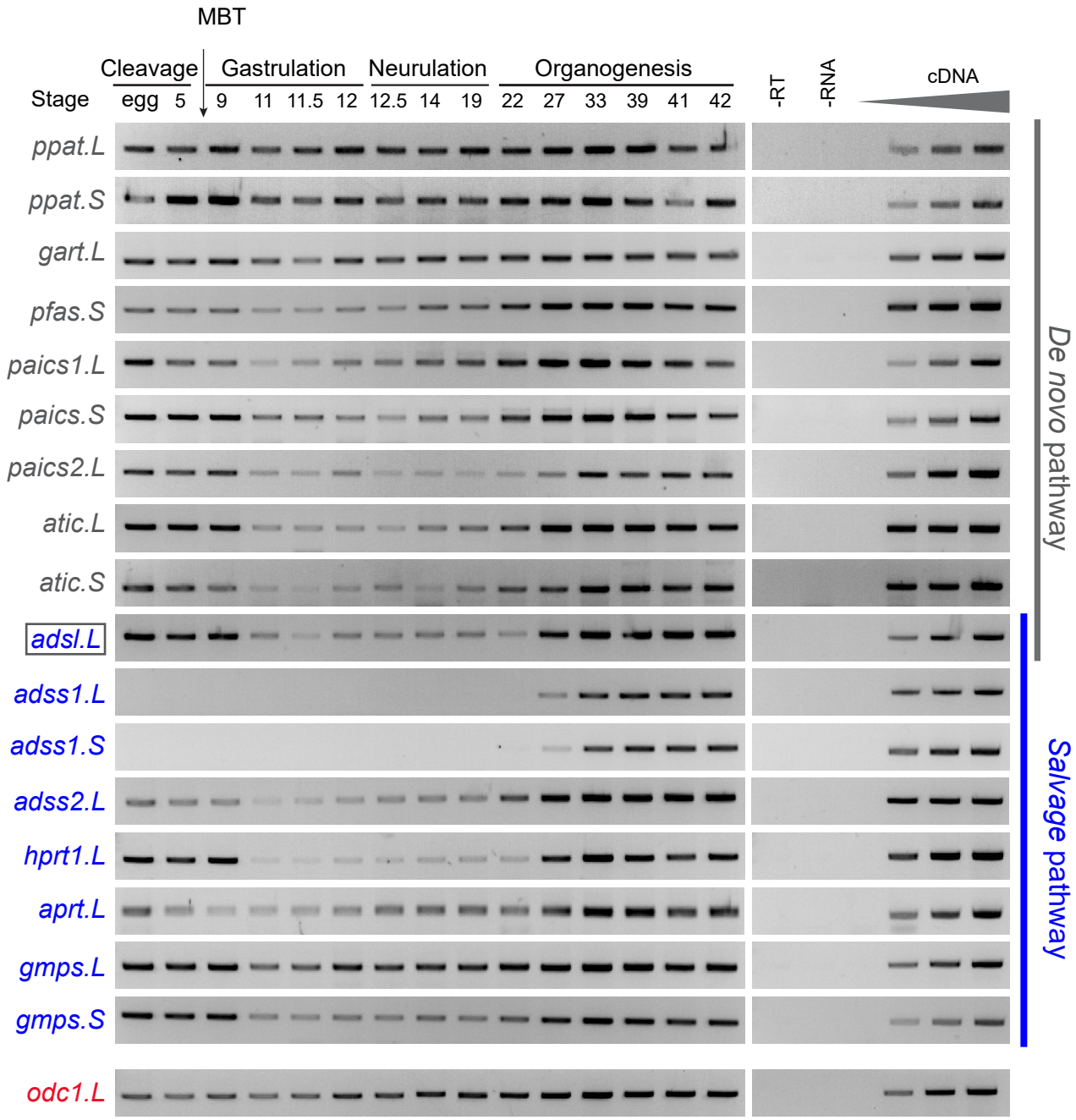

Figure S6. Temporal expression profiles of purine pathway genes during embryogenesis. The expression profile was determined for each gene by RT-PCR from cDNA of fertilized egg and whole embryo at different stages covering the different phases of *X. laevis* embryogenesis. Negative controls were performed in the absence of either reverse transcriptase (-RT) or total RNA extract (-RNA). The linearity was performed with doubling dilutions of cDNA. A loading control was done using *odc1.L* gene (in red). Names corresponding to genes encoding enzymes of the purine *de novo* and salvage pathways are written in grey and blue, respectively. The *adsl.L* gene encoding the adenylosuccinate lyase involved in both purine pathways is boxed in grey. Experiments were done at least twice ($n \geq 2$) on embryos obtained from *in vitro* fertilization of oocytes from two different females (N=2). Sense and antisense primers are described in Table S5. MBT: mid blastula transition.

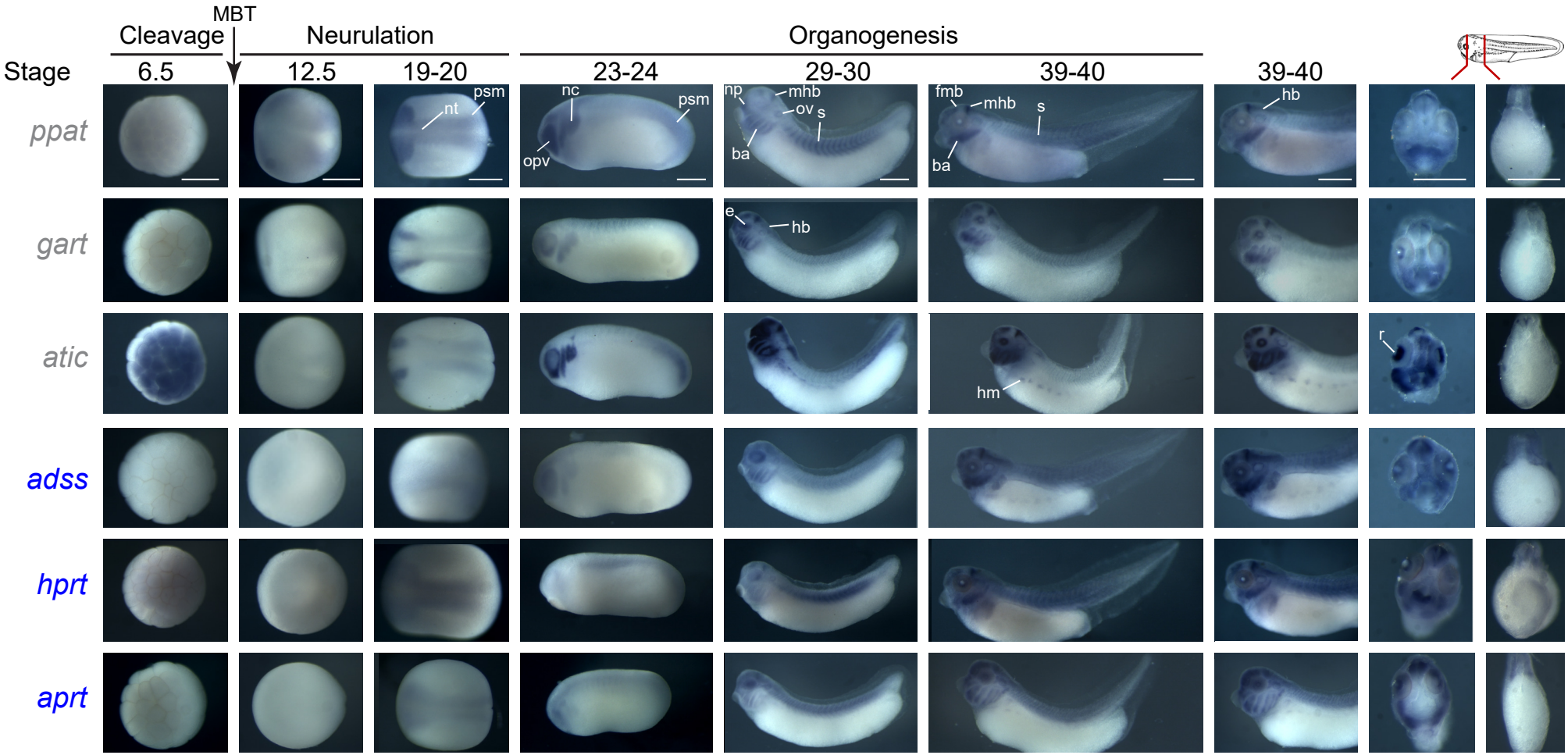

Figure S7. The expression profile was determined for each gene by *in situ* hybridization using antisense riboprobes (Table S4). No unspecific staining was detected with the control sense probes (Figure S8). MBT: Mid blastula transition. Grey and blue gene name colors refer to *de novo* and salvage purine pathways, respectively. Representative embryos were photographed. Stage 6.5: animal pole view, later stages: lateral views, with dorsal is up and anterior is left. Transverse section: dorsal is up. Abbreviations: ba, branchial arches; e, eye; fmb, forebrain-midbrain boundary; hb, hindbrain; hm, hypaxial muscles; l, lens; mhb, midbrain-hindbrain boundary; n: nasal placode; nc, neural crest; np, neural plate; nt, neural tube; opv, optical vesicle; ov, otic vesicle; psm, presomitic mesoderm; r, retina; s, somites. Bars: 0.5 mm.

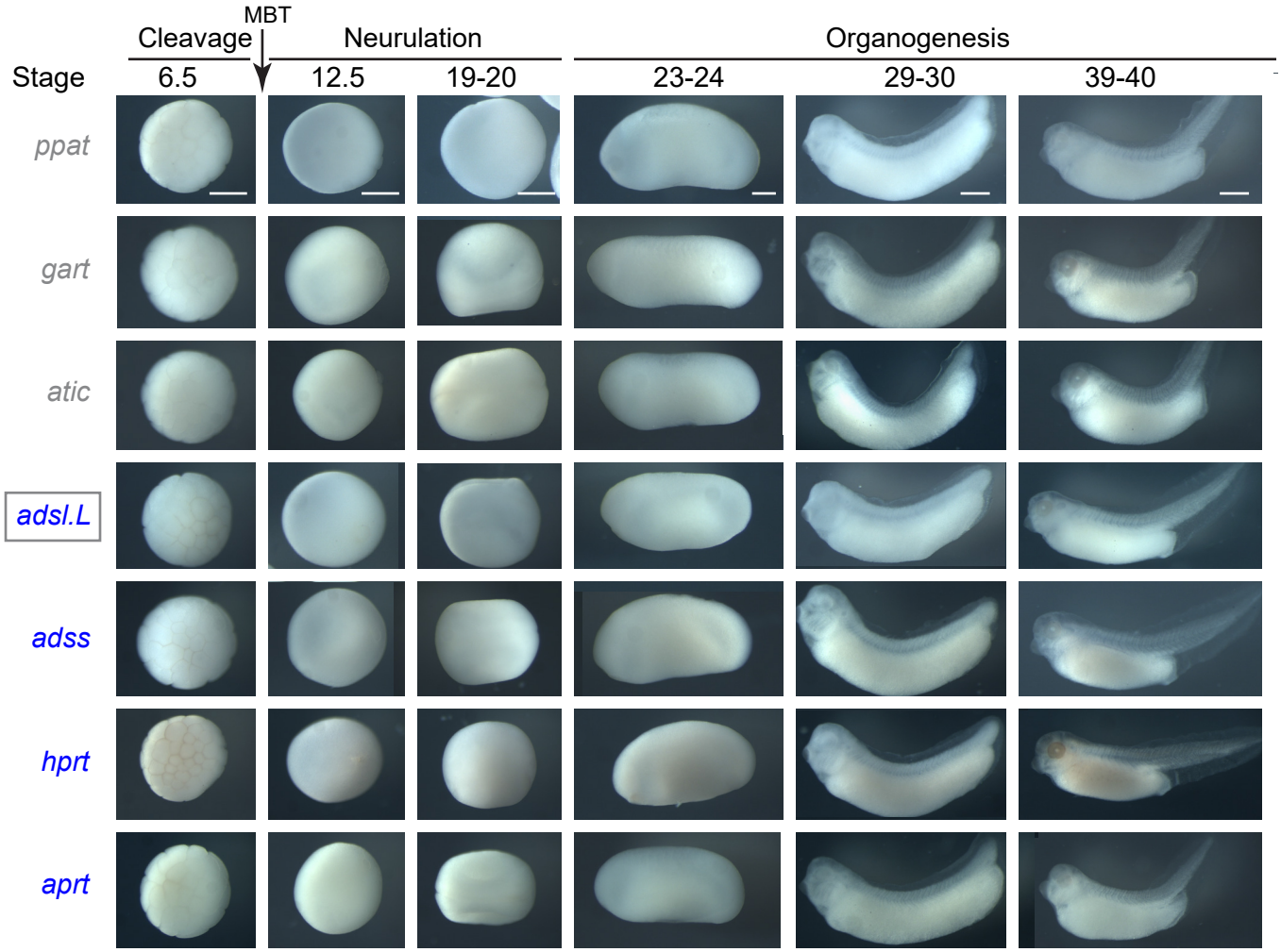

Figure S8. *In situ* hybridization using control sense riboprobes. *In situ* hybridization sense probes are described in Table S4. MBT: Mid blastula transition. Grey and blue gene name colors refer to *de novo* and salvage purine pathways, respectively. Representative embryos were photographed. Stage 6.5: animal pole view, later stages: lateral views, with dorsal is up and anterior is left. Bars: 0.5 mm.

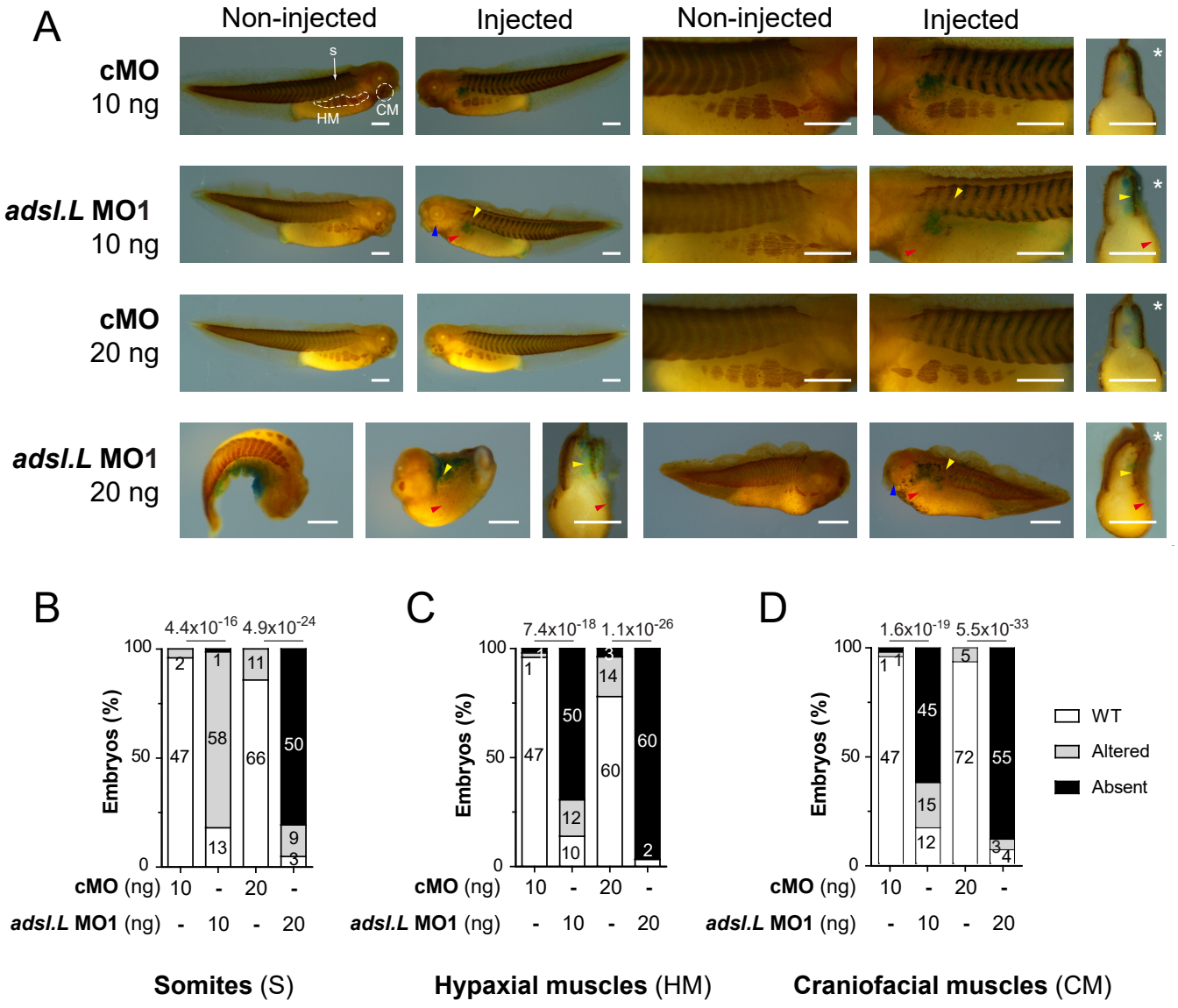

Figure S9. Severity of *adsl.L* knock-down-associated phenotypes is morpholino dose-dependent. 12-101 immunolabelling revealed a strong alteration of myogenesis and somitogenesis (**A**-**B**), hypaxial (**A**, **C**) and craniofacial (**A**, **D**) muscle formation in *adsl.L* morphant embryos. Representative images (**A**), quantification (embryo numbers in bars) and statistics of somite (**B**), hypaxial muscle (**C**) and craniofacial muscle (quadratoangularis + levator mandibularis longus) (**D**) phenotypes at tadpole stage. Yellow, blue and red arrowheads points to regions of somitic (S), craniofacial (CM) and hypaxial (HM) muscle defaults, respectively. Asterisks show injected side. Bars: 0.5 mm. Numbers above the bars in the histograms correspond to p-values.

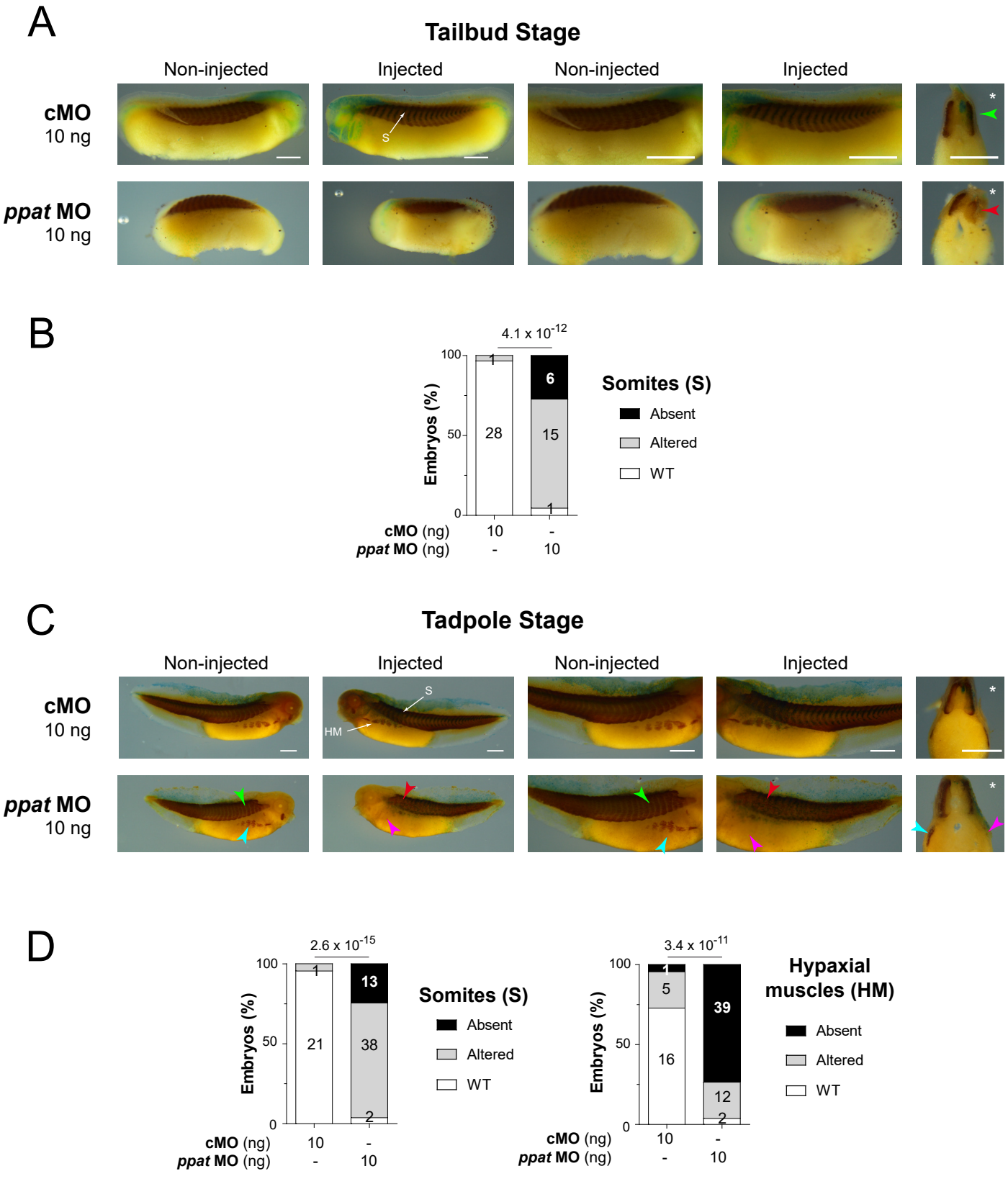

Figure S10. The *ppat.L* and *ppat.S* genes are required for somite, myotome and hypaxial muscle formation in *Xenopus laevis*. (**A-D**) A strong muscle alteration in *ppat* knock-down embryos is revealed by 12-101 immunolabelling. Representative images (**A, C**), quantification (embryo numbers in bars) and statistics (**B**, **D**) of somite and hypaxial muscle phenotypes at tailbud (**A-B**) and tadpole (**C-D**) stages. Green and red arrowheads point to normal v-shaped and altered somites, respectively; blue and pink arrowheads show normal and reduced 12/101 positive hypaxial muscle area, respectively. Injected side is indicated by asterisks. S: somites; HM: Hypaxial muscles. Bars: 0.5 mm. Numbers above the bars in the histograms correspond to p-values.

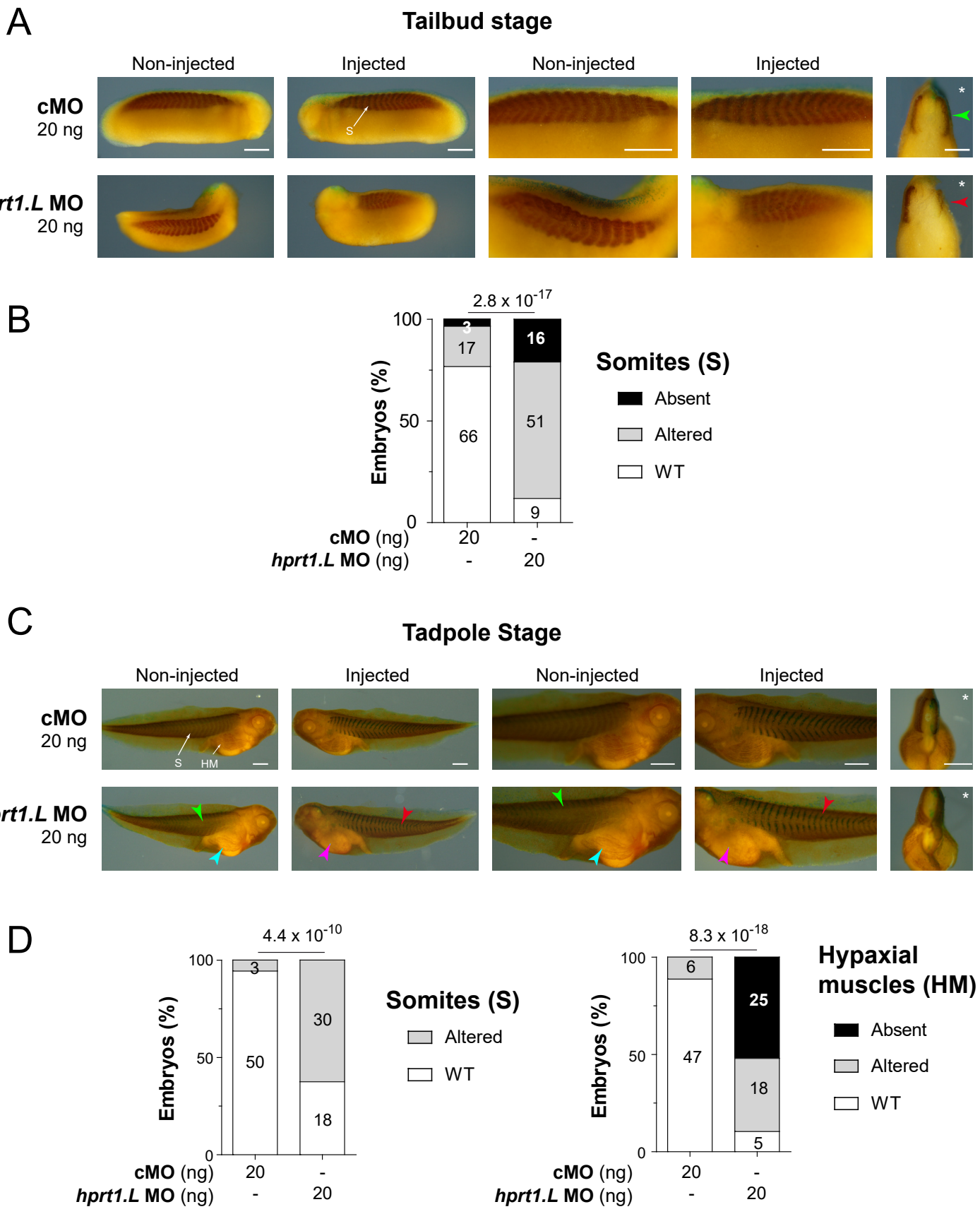

Figure S11. The *hprt1.L* gene is required for somite, myotome and hypaxial muscle formation in *Xenopus laevis*. (**A-D**) A strong muscle alteration is revealed by 12-101 immunolabelling in *hprt1.L* knock-down embryos. Representative images (**A, C**), quantification (embryo numbers in bars) and statistics (**B**, **D**) of somite and hypaxial muscle phenotypes at tailbud (**A-B**) and tadpole (**C-D**) stages. Green and red arrowheads point to normal v-shaped and altered somites, respectively; blue and pink arrowheads show normal and reduced 12/101 positive hypaxial muscle area, respectively. Injected side is indicated by asterisks. S: somites; HM: Hypaxial muscles. Bars: 0.5 mm. Numbers above the bars in the histograms correspond to p-values.

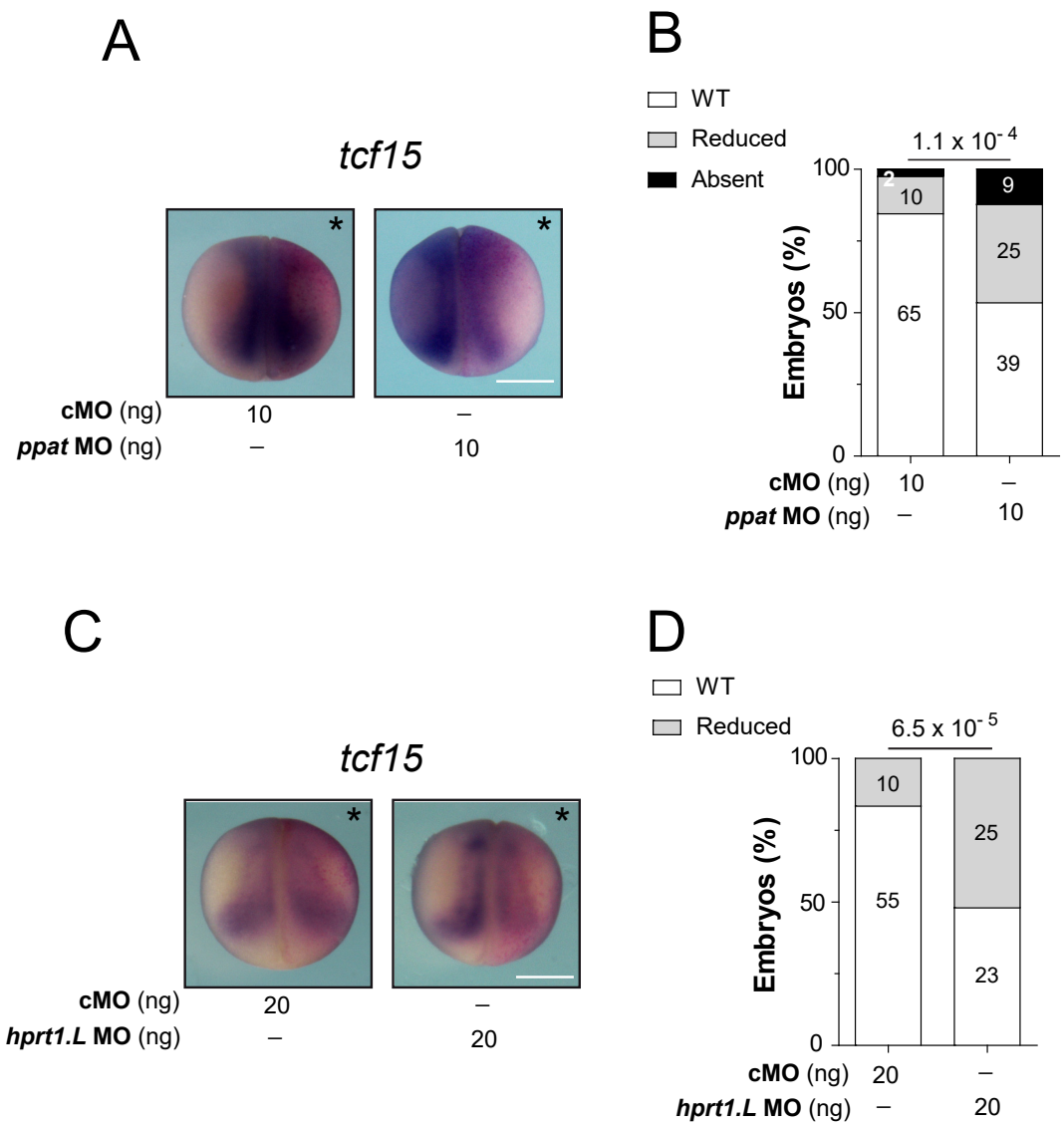

Figure S12. The *ppat.L*/*ppat.S* and *hprt1.L* genes are required for expression of *tcf15* gene. Expression of *tcf15* RNA was monitored by *in situ* hybridization at late neurula stage (stage 17-19) on embryos injected with the control morpholino (cMO) or the specific MO targeting either *ppat* or *hprt1.L* genes. Representatives images are presented for *ppat* (**A**) and *hprt1.L* (**C**) genes. Quantification (numbers in bars) and statistics of the *tcf15* expression phenotypes are presented in (**B**, **D**). Injected side is indicated by asterisks. Bars: 0.5 mm. Numbers above the bars in the histograms correspond to p-values.

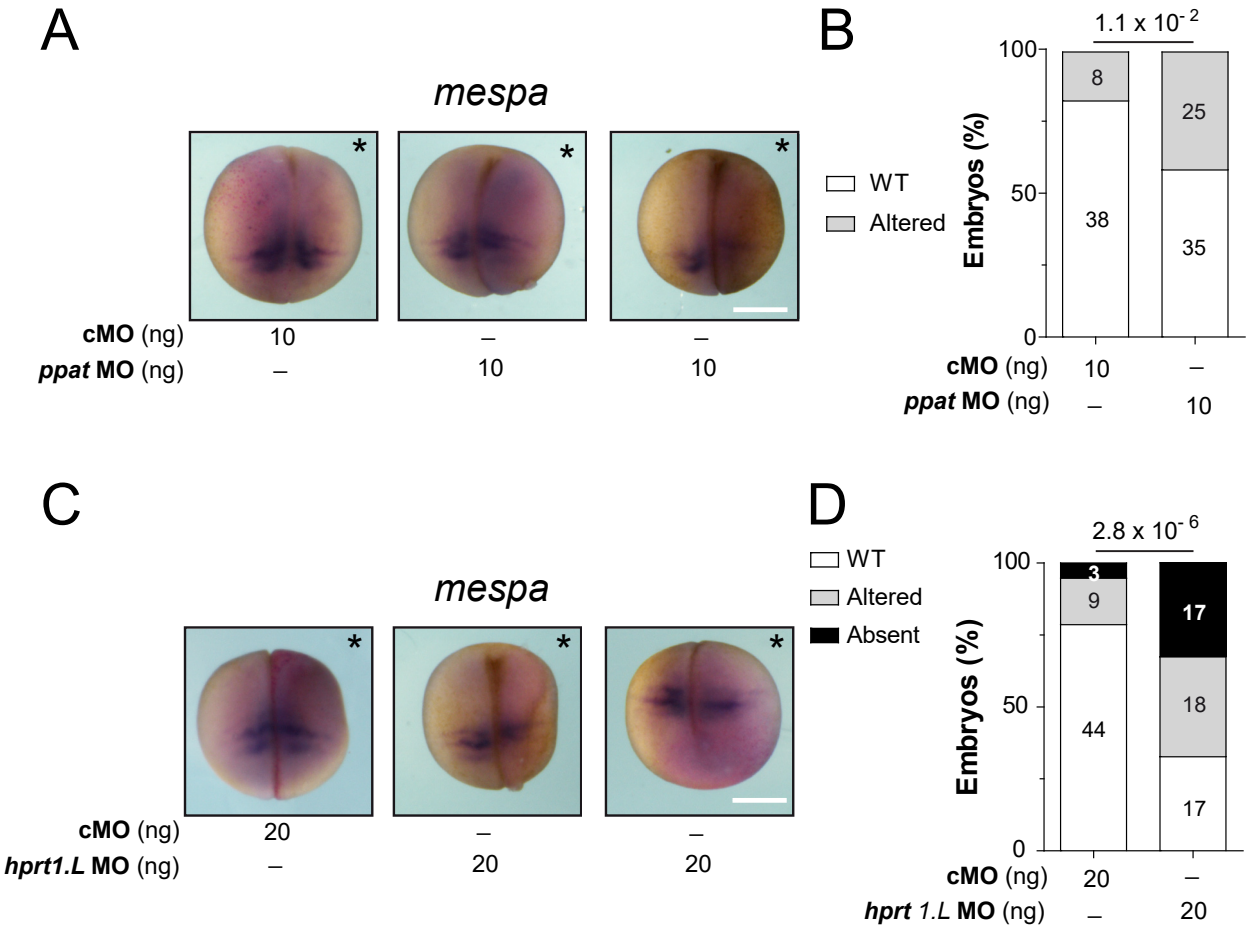

Figure S13. The *ppat.L*/*ppat.S* and *hprt1.L*genes are required for *mespa* gene expression. Expression of *mespa* RNA was monitored by *in situ* hybridization at late neurula stage (stage 17-19) on embryos injected with the control morpholino (cMO) or the specific MO targeting either *ppat* or *hprt1.L* genes. Representatives images are presented for *ppat* (**A**) and *hprt1.L* (**C**) genes, respectively. Quantification (numbers in bars) and statistics of the *mespa* expression phenotypes are presented in (**B**, **D**). Injected side is indicated by asterisks. Bars: 0.5 mm. Numbers above the bars in the histograms correspond to p-values.

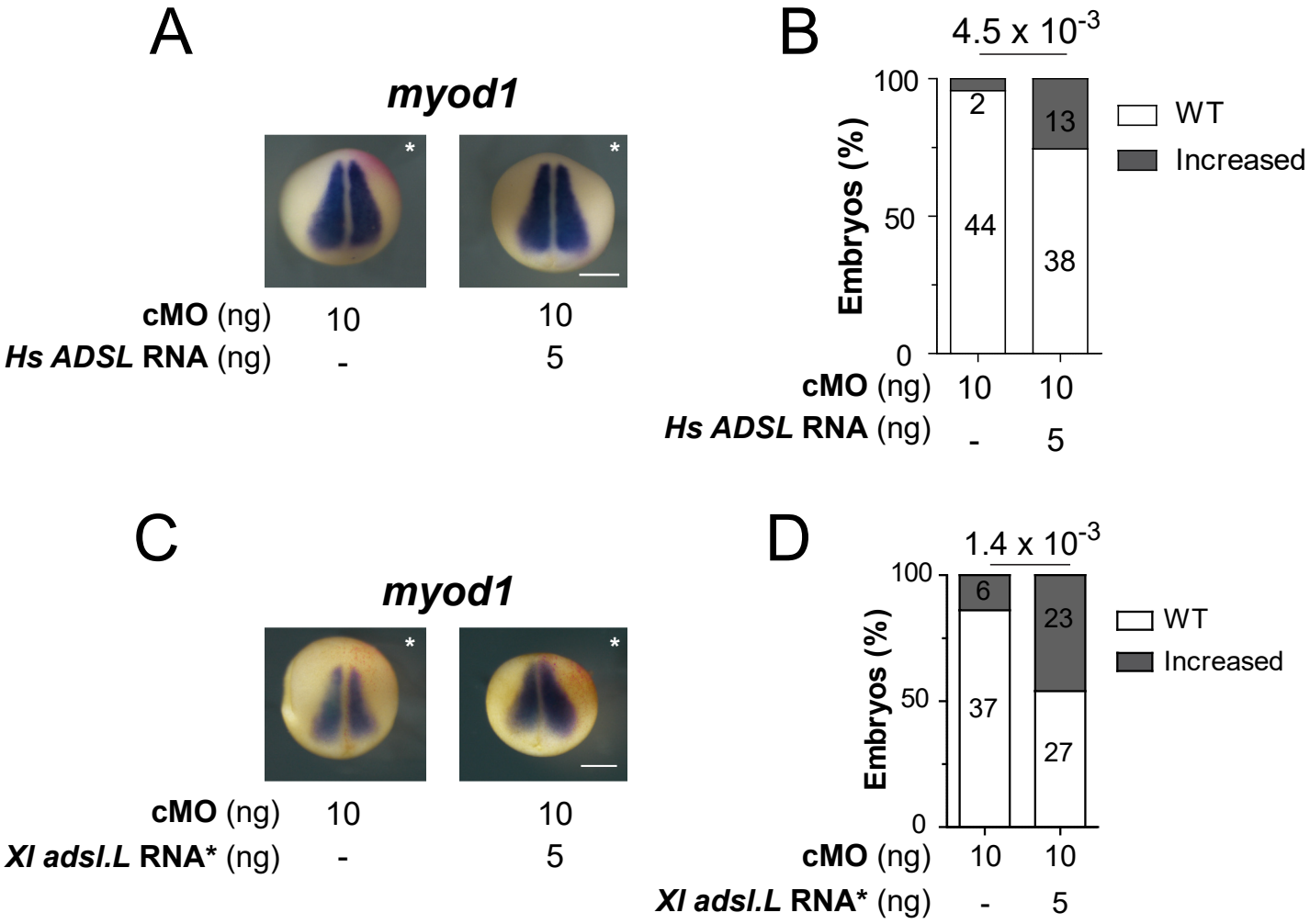

Figure S14. Effect of *H. sapiens ADSL* and *X. laevis adsl.L* RNA* on *myod1* expression at stage 12.5. (**A, C**) Expression of *myod1* was monitored by *in situ* hybridization at stage 12.5 on embryos injected with the control morpholino (cMO) and co-injected or not (-) with either the *H. sapiens ADSL* RNA (**A**) or the *X. laevis* MO non-targeted *adsl.L* RNA* (**C**), (**B, D**) Quantification (numbers in bars) and statistics of the *myod1* expression phenotypes are presented in (**A**, **C**). Injected side is indicated by asterisks. Bars: 0.5 mm. Numbers above the bars in the histograms correspond to p-values.

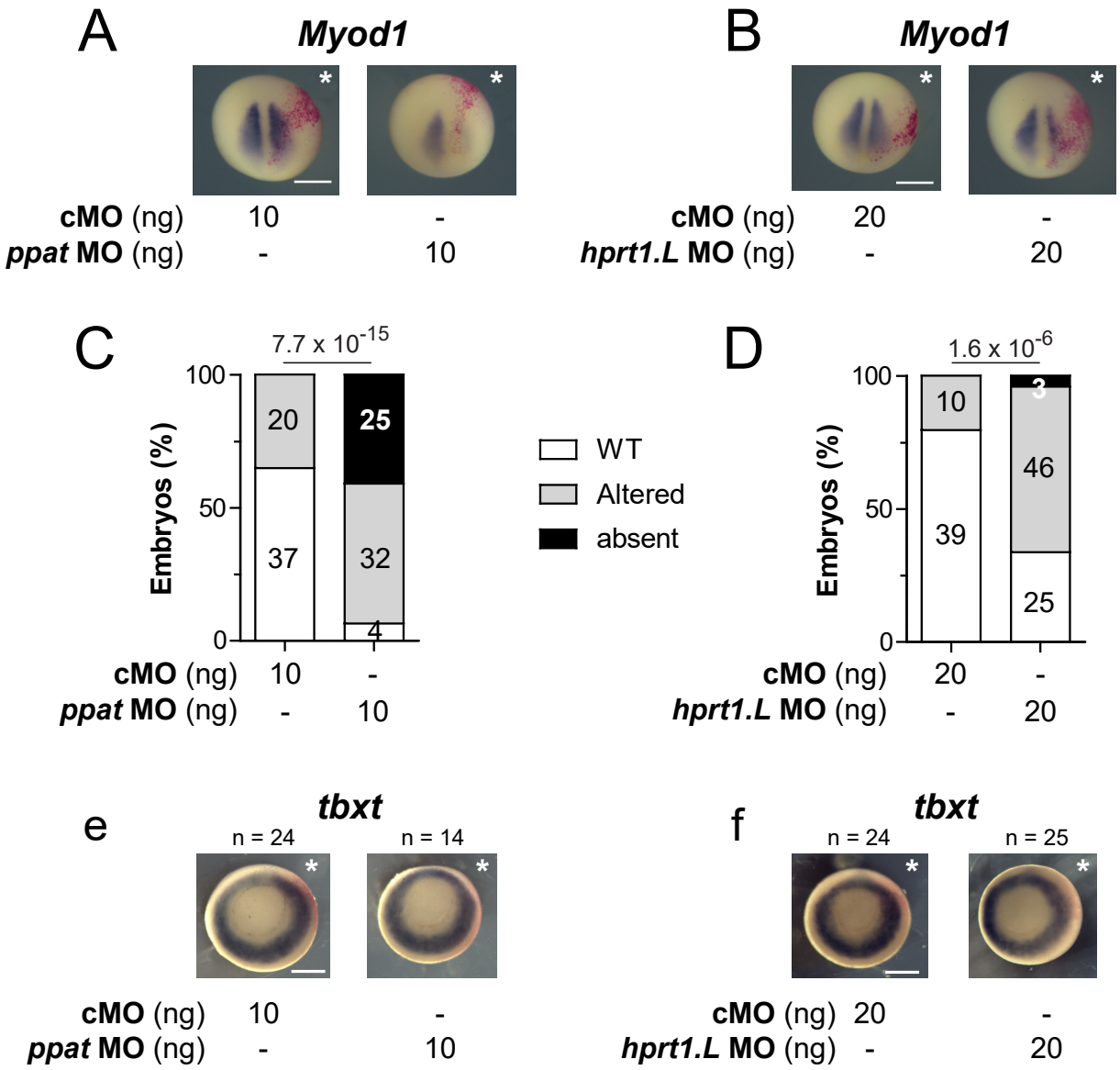

Figure S15. Expression of the myogenic regulatory factor *myod1* gene in the paraxial mesoderm is strongly affected by knock-down of *ppat* and *hprt1.L* genes. (**A-B**) Representative images of *myod1* expression alteration by the knock-down of either *ppat.L*/*ppat.S* (**A**) or *hprt1.L* (**B**) genes at stage 12.5, (**C-D**) Quantification (embryo numbers in bars) and statistics of the *myod1* expression phenotypes presented in (**A-B**). (**E-F**) Knock-down of both *ppat.L*/*ppat.S* (**E**) or *hprt1.L* (**F**) genes has no significant effect on general mesoderm formation, as revealed by the pan-mesoderm *tbxt* (*xbra*) expression pattern at stage 11. Injected side is indicated by asterisks. Bars: 0.5 mm. Numbers above the bars in the histograms correspond to p-values.

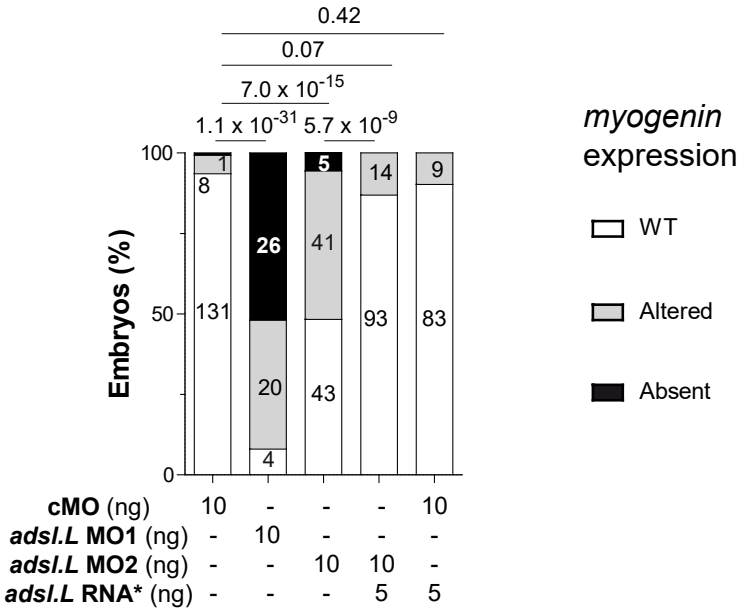

Figure S16. Statistical analysis of the effects associated with *adsl.L* knock-down on *myogenin* expression in craniofacial muscles in late tailbud stage embryos. Quantification (numbers in bars) and statistics of the *myogenin* expression phenotypes presented in Figure 6A. Numbers above the bars in the histograms correspond to p-values.

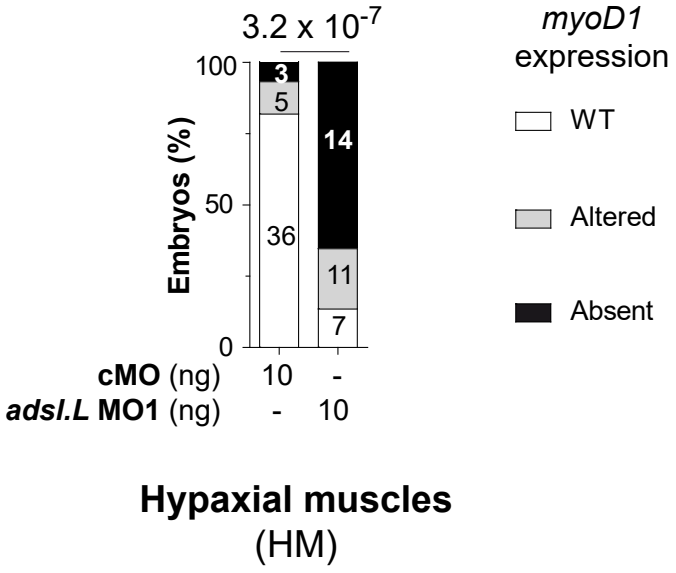

Figure S17. Statistical analysis of the effects consecutive to *adsl.L* knock-down on *myod1* expression in hypaxial muscles in late tailbud stage embryos. Quantification (numbers in bars) and statistics of the *myod1* expression phenotypes presented in Figure 5C. Numbers above the bars in the histograms correspond to p-values.

Table S1: Yeast strains

Strain	Genotype	Reference
BY4741	*Matα ura3Δ leu2Δ his3Δ lys2Δ*	Euroscarf
BY4742	*Mat**a** ura3Δ leu2Δ his3Δ met15Δ*	Euroscarf
DS1-2B/1	*Matα ura3Δ ade2 apt1 aah1*	R. Woods
Y1036	*Matα ura3Δ leu2Δ his3Δ lys2Δ ade1::kanMX4*	Lab collection
Y1057	*Matα ura3Δ leu2Δ his3Δ lys2Δ ade4::kanMX4*	Lab collection
Y1059	*Matα ura3Δ leu2Δ his3Δ lys2Δ ade5,7::kanMX4*	Lab collection
Y1063	*Matα ura3Δ leu2Δ his3Δ lys2Δ ade8::kanMX4*	Lab collection
Y1095	*Matα ura3Δ leu2Δ his3Δ lys2Δ ade16::kanMX4 ade17::kanM*	Lab collection
Y1133	*Mata ura3Δ leu2Δ his3Δ lys2Δ ade8::kanMX4*	Lab collection
Y3574	*Matα ura3Δ leu2Δ his3Δ ade1::kanMX4 ade13::kanMX4*	Lab collection
Y8093	*Matα ura3Δ leu2Δ his Δ ade2::kanMX4 hpt1::kanMX4*	Lab collection
Y11114	*Matα ura3Δ leu2Δ his3Δ lys2Δ ade2::KanMX4 ade12::HIS3*	Lab collection

Table S2: Plasmids used for functional complementation in *S. cerevisiae*

Plasmid	I.M.A.G.E Clone used for amplification	Characteristics	Reference
pCM189	N/A	*CEN ARS URA3 tet-OFF promoter*	Gari 1997[a]
p4930	IRBHp990G1167D	*CEN ARS URA3 tet-atic.L. (X. laevis)*	This study
p4933	IRBHp990H0610D	*CEN ARS URA3 tet-adsl.L. (X. laevis)*	This study
p5153	IRAKp961G14156Q	*CEN ARS URA3 tet-atic.S. (X. laevis)*	This study
p5255	IRBHp990F0459D	*CEN ARS URA3 tet-paics.1.L. (X. laevis)*	This study
p5257	IRBHp990G071D	*CEN ARS URA3 tet-paics.1.S. (X. laevis)*	This study
p5303	IRBHp990C0135D	*CEN ARS URA3 tet-adss.1.S. (X. laevis)*	This study
p5304	IRBHp990B1280D	*CEN ARS URA3 tet-adss.1.L. (X. laevis)*	This study
P5318	IRBH990B02030D	*CEN ARS LEU2 tet-hprt.L (X. laevis)*	This study
p5321	IRAKp961E17253Q	*CEN ARS URA3 tet-aprt.L (X. laevis)*	This study
p5551	IRBHp990H1017D	*CEN ARS URA3 tet-ppat.L.(X. laevis)*	This study
p5400	IMAGp998O0914583Q	*CEN ARS URA3 tet-ppat.S (X. laevis)*	This study
p5550	IRBH990B02030D	*CEN ARS LEU2 tet-hprt.S (X. laevis)*	This study
p5697	IRAKp961P06157Q	*CEN ARS URA3 tet-paics.2 (X. laevis)*	This study
p5740	IMAGp998B1011965Q	*CEN ARS URA3 tet-gart (X. tropicalis)*	This study
P5744	IMAGp998B1011965Q	*CEN ARS URA3 tet-gars (X. tropicalis)*	This study
P5269	IRAKp961C16299Q	*CEN ARS LEU2 tet-airs (X. laevis)*	This study

[a] E Garí, L Piedrafita, M Aldea, E Herrero A set of vectors with a tetracycline-regulatable promoter system for modulated gene expression in Saccharomyces cerevisiae **1997** *Yeast* 13(9):837-48. DOI: 10.1002/(SICI)1097-0061(199707)13:9<837::AID-YEA145>3.0.CO;2-T

Table S3: Plasmids used for capped mRNA synthesis.
Linear. Enzyme: restriction enzyme used for linearization. *Hs: Homo sapiens*. * refers to morpholinos non-targeted sequences.

mRNA	Linear. Enzyme	Plasmids
ads1.L	*Xho*I	IRBHp990H0610D
*ads1.L**	*Xho*I	pBF-*adsl.L** from IRBHp990H0610D
Hs ADSL	*Not*I	pCS2^{+}-HsADSL
ppat.L	*Xba*I	IRBHp990H1017D
*ppat.L**	*Sal*I	pBF-*ppat.L** from IRBHp990H1017D
ppat.S	*Hind*III	IMAGp998O0914583Q
*ppat.S**	*Xho*I	pBF-*ppat.S** from IMAGp998O0914583Q
hprt1.L	*Not*I	IRBH990B02030D
*hprt1.L**	*Sac*I	pBF-*hprt1.L** from IRBH990B02030D
LacZ	*Xho*I	pSP6nucβgal

Table S4: Ribonucleotides probes used for *in situ* hybridization.
CDS: coding sequence. Linear. Enzyme : restriction enzyme used for linearization. pSK: p-BlueScript plasmid. RNA Pol.: RNA polymerase. UTR: untranslated region

Targeted genes	Probe	Linear. Enzyme	RNA Pol.	Plasmids
adsl.L	sense	*Kpn*I	T7	p5265 *adsl.L*-pSK (CDS +3'UTR; 480 bp) from IRBHp990H0610D
	antisense	*Sac*I	T3	p5265 *adsl.L*-pSK (CDS +3'UTR; 480 bp) from IRBHp990H0610D
adss1.L *adss1.S*	sense	*Sac*I	T3	p5634 *adss1.L*-pSK (5'UTR + CDS; 444 bp) from IRBHp990C0135D
	antisense	*Sal*I	T7	p5634 *adss1.L*-pSK (5'UTR + CDS; 444 bp) from IRBHp990C0135D
adss2.L	sense	*SacI*	T3	p5428 *adss2.L*-pKS (5'UTR + CDS; 444 bp) from IRBHp990E047D
	antisense	SalI	T7	p5428 *adss2.L*-pKS (5'UTR + CDS; 444 bp) from IRBHp990E047D
aprt.L	sense	*Kpn*I	T7	p5435 *aprt.L*-pKS (CDS +3'UTR; 779 bp) from IRAKp961E17253Q
	antisense	*Eco*RV	T3	p5435 *aprt.L*-pKS (CDS +3'UTR; 779 bp) from IRAKp961E17253Q
atic.L *atic.S*	sense	*Xho*I	SP6	P4915 *atic.L*-pExpress1 (CDS +3'UTR; 1854 bp) from IRBHp990G1167D
	antisense	*Eco*RI	T7	P4915 *atic.L*- pExpress1 (CDS +3'UTR; 1854 bp) from IRBHp990G1167D
hprt.L	sense	*Ase*I	T7	p5454 *hprt.L*-pKS (5'UTR + CDS; 592 bp) from IRBH990B02030D
	antisense	*Sac*I	T3	p5454 *hprt.L*-pKS (5'UTR + CDS; 592 bp) from IRBH990B02030D
gart.L	sense	*Bam*HI	T3	p5426 *gart.L*-pKS (CDS +3'UTR ; 530 bp) from IRAKp961C16299Q
	antisense	*Eco*RV	T7	p5426 *gart.L*-pKS (CDS +3'UTR ; 530 bp) from IRAKp961C16299Q
ppat.L *ppat.S*	sense	*Not*I	T3	p5527 *ppat.L*-pSK (CDS ; 481 bp) from XL.29008
	antisense	*Eco*RV	T7	p5527 *ppat.L*-pSK (CDS ; 481 bp) from XL.29008

Table S5: Oligonucleotides used for RT-PCR analyses. Amplification temperature and number of RT-PCR cycles were determined to obtain a single PCR product.

Amplified gene	Sense oligonucleotide (5'-3')	Antisense oligonucleotide (5'-3')	Amplification Temperature (°C)	Nb of cycles
ppat.L	GTTAGTCCCTGTGGCCGCT	GCCCATGCCCTTGTGCATTC	54	28
ppat.S	GAAGCGCGAGGTGTGTGTG	GCCCATGCCCTTGTGCATTC	58	29
gart.L	CAGAGACAGTTCTAGTGATTGG	GATAATCCCTGCTGCCAGAG	56	29
pfas.S	CTGACAGAACGTGCAGGG	CTAGTCTGGAACTTTATGAG	53	29
paics.1.S	CAGAACCACGTGGTACTGCC	GATCCCAGCCTCCTGCAGC	56	30
paics.1.L	GAAATGGAGTCTTACGCAGAAC	GATCCCAGCCTCCTGCAGC	53	27
paics.2.L	GCATTTGTTAAGAGGTGCAG	CCAAACTTAATCCTCATGTCC	55	28
adsl.L	ATGGCCTTCAACTTCAGCGA	AACGTTGGCATCTCTGCGTA	55	28
atic.L	GCTGCTAGCGACTTTATCCAG	GGGTACAGGTTACACACAAC	57	31
atic.S	GCTGTTTGCGGAGATGGAG	GGGTACAGGTTACACACAAC	53	30
adss1.L	CAAGTGGCATTATCAACCCC	CTTTGGATGAATATGTTGGTC	51	30
adss1.S	GTGGCATTATAAATCCTAAAGC	CTTTGGATGAATATGTTGGTC	53	29
Adss2.L	CCGCTACAGTAAGCGTAAC	GCTTTCATAGGAAATGGTGTG	51	28
hprt1.L	CTAAACATTATGCAGCCGATC	CATTCTTGCCTGTCAAGGTGG	54	26
hprt1.S	CTAAACACTACGCCGCCAGC	CATTCTTGCCTGTCAAGGTGG	52	29
aprt.L	CAGATTATGTCCGATCAGGAG	GCTAACAGATTCTGTGGGAC	57	29
gmps.L	GAGCGATGGGCAGAGATC	CTGTAAGAGCGACAGTCC	56	28
gmps.S	GAGGGTTGGGTAGAGAAC	CTGTAAGAGCGACAGTCC	53	29
odc1.L	GTCAATGATGGAGTGTATGGATC	TCCATTCCGCTCTCCTGACCAC	55	23

Table S6: Comparison of the purine biosynthesis pathways encoding genes and proteins between, *X. laevis*, *H. sapiens* and *X. tropicalis*. Alignments were performed using https://blast.ncbi.nlm.nih.gov. * XB: xenbase: https://www.xenbase.org/entry/

Xenopus laevis			***Homo sapiens***				***Xenopus tropicalis***				
Protein name	**Accession Number**	**XB* Gene ID**	**Protein name**	**Accession Number**	**Identity %**	**Coverage %**	**Protein name**	**Accession Number**	**Identity %**	**Coverage %**	**Enzymatic activity**
Ada.L	XP_018090401.1	17336388	ADA	NP_000013.2	74	97	Ada	NP_001011025.1	97	100	Adenosine deaminase
Ada.S	NP_001085740.1	950506			70	98					
Ada2.L	NP_001090531.1	6254244	ADA2	NP_001269154.1	57	96	Ada2	XP_031754454.1	90	99	Adenosine deaminase
Ada2.S	NP_001089165	6251688	ADA2		59	97	Ada2		88	100	
Ada.2.S	NP_001087740.1	5929096	ADA.2	No significant homolog			Ada.2	NP_001107369.1	90	100	Adenosine deaminase
Adk.S	NP_001086357.1	997231	ADK	NP_001114.2	82	95	Adk	NP_001016698	98	99	Adenosine kinase
Adsl.L	NP_001080593	380285	ADSL	NP_000017.1	83	93	Adsl	NP_001005457.1	96	100	Adenylosuccinate lyase
Adssl1.L	NP_001090012.1	5758296	ADSS1	NP_689541.1	88	100	Adssl1	NP_001004939.1	97	100	Adenylosuccinate synthase
Adssl1.S	NP_001087505.1	6254009	ADSS1		87	100	Adssl1		96	100	
Adss2.L	NP_001080088.1	944129	ADSS2	NP_001117.2	86	94	Adss2	NP_989047.1	95	100	Adenylosuccinate synthase
Ak1.L	NP_001087683.1	6253770	AK1	NP_001305051.1	74	98	Ak1	NP_001006817.1	91	97	Adenylate kinase
Ak1.S	NP_001085451.1	6251725	AK1		81	98	Ak1		100	100	
Ak2.L	XP_018102289.1	17344313	AK2	NP_001616.1	82	100	Ak2	XP_012812152.1	96	100	Adenylate kinase
Ak2.S	NP_001080232.1	6254479	AK2		79	100	Ak2		97	100	
Ak3.L	NP_001089446.1	977031	AK3	NP_057366.2	74	97	Ak3	XP_012812420.1	90	100	Adenylate kinase
Ak3.S	NP_001084561.1	17332462	AK3		75	97	Ak3		92	100	
Ak4.L	XP_018113718.1	17341782	AK4	NP_001005353.1	77	96	Ak4	XP_002931643.1	96	100	Adenylate kinase
Ak4.S	XP_018116248.1	959957			74	94	Ak4		97	100	
Ak5.L	XP_018113675.1	6487811	AK5	AAH36666.1	72	100	Ak5	XP_012815974.2	93	100	Adenylate kinase
Ak5.S	XP_018116212.1	17345311	AK5	NP_777283.1	71	100	Ak5		92	100	
Ak6.L	NP_001089528.1	972297	AK6	NP_057367.1	76	100	Ak6	NP_001017167.1	95	100	Adenylate kinase
Ak6.S	NP_001087040.1	17335043	AK6		78	100	Ak6		97	100	

Ak7.S	NP_001081046.1	953552	AK7	NP_689540.2	63	99	Ak7	NP_001011352.1	93	100	Adenylate kinase
Ak8.L	NP_001088862.1	5831351	AK8	NP_689785.1	55	98	Ak8	NP_989104.1	90	100	Adenylate kinase
Ak9.L	XP_018118807	17335922	AK9	NP_001316531.1	52	34	Ak9	XP_031757751.1	85	96	Adenylate kinase
Ak9.S	XP_018118808	17335923	AK9		52	34	Ak9		85	96	
Ampd1.L	XP_018101841.1|	17335636	AMPD1	NP_000027.2	74	99	Ampd1	XP_002935821.2	95	100	Adenosine monophosphate deaminase
Ampd1.S	XP_018104675.1	17335637	AMPD1		72	99	Ampd1		92	100	
Ampd2.S	XP_018104829	6489067	AMPD2	NP_001355738.1	80	96	Ampd2	XP_031752724.1	96	100	Adenosine monophosphate deaminase
Ampd3.L	XP_018112762.1	6489056	AMPD3	NP_000471.1	80	99	Ampd3	NP_001025687.1	94	100	Adenosine monophosphate deaminase
Ampd3.S	XP_018115800.1	17344991	AMPD3		80	99	Ampd3		95	100	
Aprt.L	XP_018096991.1	6253243	APRT	NP_000476.1	65	100	Aprt	NP_001007941.1	93	100	Adenine phosphoribosyltransferase
Atic.L	NP_001090100.1	998812	ATIC	NP_004035.2	78	99	Atic	NP_001005460.1	95	100	Amino-Imidazole CarboxAmide Ribonucleotide transformylase and IMP cyclohydrolase
Atic.S	XP_018094436.1	17331460	ATIC		79	99	Atic		96	100	
Gda.L	NP_001083074.1	987047	GAH	NP_004284.1	61	93	Gda	XP_004910825.1	93	96	Guanine deaminase
Gda.S	XP_018099342.1	17337222	GAH		60	99	Gda		83	99	
Gart.L	NP_001093352.1	6251947	GART	NP_000810.1	75	98	Gart	XP_012813454.1	92	98	Phosphoribosylglycinamide-formyltransferase, phosphoribosylglycinamide synthetase and phosphoribosylaminoimidazole synthetase
Gmps.L	XP_018119259.1	950699	GMPS	NP_003866.1	92	98	Gmps	XP_002933290.3	97	98	Guanine monophosphate synthase
Gmps.S	XP_018121231.1	17340569	GMPS		93	100	Gmps		98	100	
Guk1.L	NP_001087146.1	6254574	GUK	NP_000849.1	70	97	Guk1	NP_001034818.1	89	100	Guanylate kinase
Guk1.S	NP_001086807.1	17334557	GUK		69	97	Guk1		90	100	
Hprt1.L	NP_001090235.1	6078713	HGPRT	NP_000185.1	89	99	Hprt1	NP_989312.1	100	100	Hypoxanthine-Guanine phosphorybosyl transferase
Impdh1.L	NP_001080792	957455	IMPDH1	NP_000874.2	92	100	Impdh1	NP_001017283.1	98	100	Inosine monophosphate dehydrogenase
Impdh2.L	NP_001083990.1	17345296	IMPDH2	NP_000875.2	93	100	Impdh2	NP_001008066.1	98	100	Inosine monophosphate dehydrogenase
Impdh2.S	NP_001082410.1	478732	IMPDH2		93	100	Impdh2		97	100	
Paics.1.L	NP_001080163	17334793	PAICS	NP_001072992.1	81	100	Paics.1	XP_012811124.2	96	100	Phosphoribosylaminoimidazole carboxylase Phosphoribosylaminoimidazolesuccino-carboxamide synthetase
Paics.1.S	NP_001086248.1	965998	PAICS		82	98	Paics.1		95	100	

Paics.2.L	XP_018085590.1	5872998	PAICS	NP_001072992.1	57	37	Paics.2	NP_001090685.1	86	97	Phosphoribosylaminoimidazole carboxylase Phosphoribosylaminoimidazolesuccino-carboxamide synthetase
Pfas.S	XP_018094887.1	6485675	PFAS	NP_036525.1	65	99	Pfas	XP_012825646.2	93	99	Phosphoribosylformylglycinamidine synthase
Pnp.L	NP_001079809.1	1011603	PNP	NP_000261.2	68	95	Pnp	NP_001006720.1	88	98	Purine nucleoside phosphorylase
Pnp.S	XP_018099448.1	17337633	PNP		66	93	Pnp		90	100	
Ppat.L	NP_001083491.1	972209	GPAT	NP_002694.3	80	100	Ppat	NP_989313.1	96	100	Phosphoribosylpyrophosphate amidotransferase
Ppat.S	XP_041435416	17340761	GPAT		79	99	Ppat		96	100	
Xdh.L	XP_018117710.1	6485774	XDH	NP_000370.2	70	99	Xdh	XP_031758260.1	89	100	Xanthine dehydrogenase/oxidase
Xdh.S	XP_018120131.1	17331587	XDH		70	92	Xdh		90	100	

Table S7: Comparison of the purine biosynthesis pathways encoding genes and proteins between *X. laevis* and *S. cerevisiae*. Alignments were performed using https://blast.ncbi.nlm.nih.gov. * XB: xenbase: https://www.xenbase.org/entry/.

[a] No significant alignment between the yeast and *X. Laevis* Hprt1.L entire sequences.

ada: adenine deaminase; xdh: xanthine dehydrogenase/oxidase

Xenopus laevis			***Saccharomyces cerevisiae***					
Protein name	**Accession Number**	**XB* Gene ID**	**Protein name**	**Accession Number**	**Identity %**	**SGD Locus ID**	**Coverage %**	**Enzymatic activity**
Ada.L Ada.S	XP_018090401.1 NP_001085740.1	17336388 950506		No Ada activity in S.c.				Adenosine deaminase
Ada2.L Ada2.S	NP_001090531.1 NP_001089165	6254244 6251688		No Ada activity in S.c.				Adenosine deaminase
Ada.2.S	NP_001087740.1	5929096	ADA.2	No Ada activity in S.c.				Adenosine deaminase
Adk.S	NP_001086357.1	997231	Ado1	NP_012639.1	40	*YJR105W*	91	Adenosine kinase
Adsl.L	NP_001080593	380285	Ade13	NP_013463.1	64	*YLR359W*	92	Adenylosuccinate lyase
Adssl1.L Adssl1.S	NP_001090012.1 NP_001087505.1	5758296 6254009	Ade12	NP_014179.1	57 57	*YNL220W*	92 92	Adenylosuccinate synthase
Adss2.L	NP_001080088.1	944129	Ade12	NP_014179.1	56	*YNL220W*	92	Adenylosuccinate synthase
Ak1.L Ak1.S	NP_001087683.1 NP_001085451.1	6253770 6251725	Adk1	NP_010512.1	28 28	*YDR226W*	84 92	Adenylate kinase
Ak2.L Ak2.S	XP_018102289.1 NP_001080232.1	17344313 6254479	Adk1	NP_010512.1	55 59	*YDR226W*	94 90	Adenylate kinase
Ak3.L Ak3.S	NP_001089446.1 NP_001084561.1	977031 17332462	Adk2	NP_011097.3	46 45	*YER170W*	86 86	Adenylate kinase
Ak4.L	XP_018113718.1	17341782	Adk2	NP_011097.3	43	*YER170W*	83	Adenylate kinase

Ak4.S	XP_018116248.1	959957			46		83	
Ak5.L Ak5.S	XP_018113675.1 XP_018116212.1	6487811 17345311	Adk2	NP_011097.3	27 25	*YER170W*	61 58	Adenylate kinase
Ak6.L Ak6.S	NP_001089528.1 NP_001087040.1	972297 17335043		none				Adenylate kinase
Ak7.S	NP_001081046.1	953552	Adk1	NP_010512.1	29	*YDR226W*	16	Adenylate kinase
Ak8.L	NP_001088862.1	5831351		none				Adenylate kinase
Ak9.L Ak9.S	XP_018118807 XP_018118808	17335922 17335923	Adk1	NP_010512.1	24 24	*YDR226W*	14 14	Adenylate kinase
Ampd1.L Ampd1.S	XP_018101841.1| XP_018104675.1	17335636 17335637	Amd1	NP_013677.1	51 51	*YML035C*	68 68	Adenosine monophosphate deaminase
Ampd2.S	XP_018104829	6489067	Amd1	NP_013677.1	53	*YML035C*	82	Adenosine monophosphate deaminase
Ampd3.L Ampd3.S	XP_018112762.1 XP_018115800.1|	6489056 17344991	Amd1	NP_013677.1	55 48	*YML035C*	64 80	Adenosine monophosphate deaminase
Aprt.L	XP_018096991.1	6253243	Apt1	NP_013690.1	47	*YML022W*	93	Adenine phosphoribosyltransferase
Atic.L Atic.S	NP_001090100.1 XP_018094436.1	998812 17331460	Ade17 Ade16 Ade17 Ade16	NP_013839.1 NP_013128.1 NP_013839.1 NP_013128.1	62 62 61 62	*YMR120C* *YLR028C* *YMR120C* *YLR028C*	99 99 99 99	Amino-Imidazole CarboxAmide Ribonucleotide transformylase and IMP cyclohydrolase
Gda.L Gda.S	NP_001083074.1 XP_018099342.1	987047 17337222	Gud1	NP_010043.1	39 39	*YDL238C*	96 91	Guanine deamnase
Gart.L	NP_001093352.1	6251947	Ade5,7 Ade8	NP_011280.1 NP_010696.3	46 29	*YGL234W* *YDR408C*	96 31	Phosphoribosylglycinamide formyltransferase, phosphoribosylglycinamide synthetase and phosphoribosylaminoimidazole synthetase
Gmps.L Gmps.S	XP_018119259.1 XP_018121231.1	950699 17340569	Gua1	NP_013944.1 NP_013944.1	37 36	*YMR217W*	93 94	Guanine monophosphate synthase

Guk1.L Guk1.S	NP_001087146.1 NP_001086807.1	6254574 17334557	Guk1	NP_010742.1	55 55	*YDR454C*	92 92	Guanylate kinase
Hprt1.L	NP_001090235.1	6078713	Hpt1	NP_010687.3	34[a]	*YDR399W*	20[a]	Hypoxanthine-Guanine phosphorybosyl transferase
Impdh1.L	NP_001080792	957455	Imd2 Imd3 Imd4	NP_012088.3 NP_013536.3 NP_013656.1	60 63 63	*YHR216W* *YLR432W* *YML056C*	97 97 97	Inosine monophosphate dehydrogenase
IImpdh2.L IImpdh2.S 	NP_001083990.1 NP_001082410.1	17345296 478732	Imd2 Imd3 Imd4 Imd2 Imd3 Imd4	NP_012088.3 NP_013536.3 NP_013656.1 NP_012088.3 NP_013536.3 NP_013656.1	61 64 63 62 64 63	*YHR216W* *YLR432W* *YML056C* *YHR216W* *YLR432W* *YML056C*	96 96 98 96 96 97	Inosine monophosphate dehydrogenase
Paics.1.L Paics.1.S	NP_001080163 NP_001086248.1	17334793 965998	Ade1 Ade2 Ade1	NP_009409.1 NP_014771.3 NP_009409.1	25 31 26	*YAR015W* *YOR128C* *YAR015W*	51 29 51	Phosphoribosylaminoimidazole carboxylase phosphoribosylaminoimidazolesuccinocarboxamide synthetase
Paics.2.L	XP_018085590.1	5872998	Ade2	NP_014771.3	31	*YOR128C*	14	Phosphoribosylaminoimidazole carboxylase phosphoribosylaminoimidazolesuccinocarboxamide synthetase
Pfas.S	XP_018094887.1	6485675	Ade6	NP_011575.1	37	*YGR061C*	93	Phosphoribosylformylglycinamidine synthase
Pnp.L Pnp.S	NP_001079809.1X P_018099448.1	1011603 17337633	Pnp1	NP_013310.1	52 45	*YLR209C*	87 91	Purine nucleoside phosphorylase
Ppat.L Ppat.S	NP_001083491.1 XP_041435416	972209 17340761	Ade4	NP_014029.1	36 36	*YMR300C*	91 92	Phosphoribosylpyrophosphate amidotransferase
Xdh.L Xdh.S	XP_018117710.1 XP_018120131.1	6485774 17331587		No Xdh activity in *S.cerevisiae*.				Xanthine dehydrogenase/oxidase